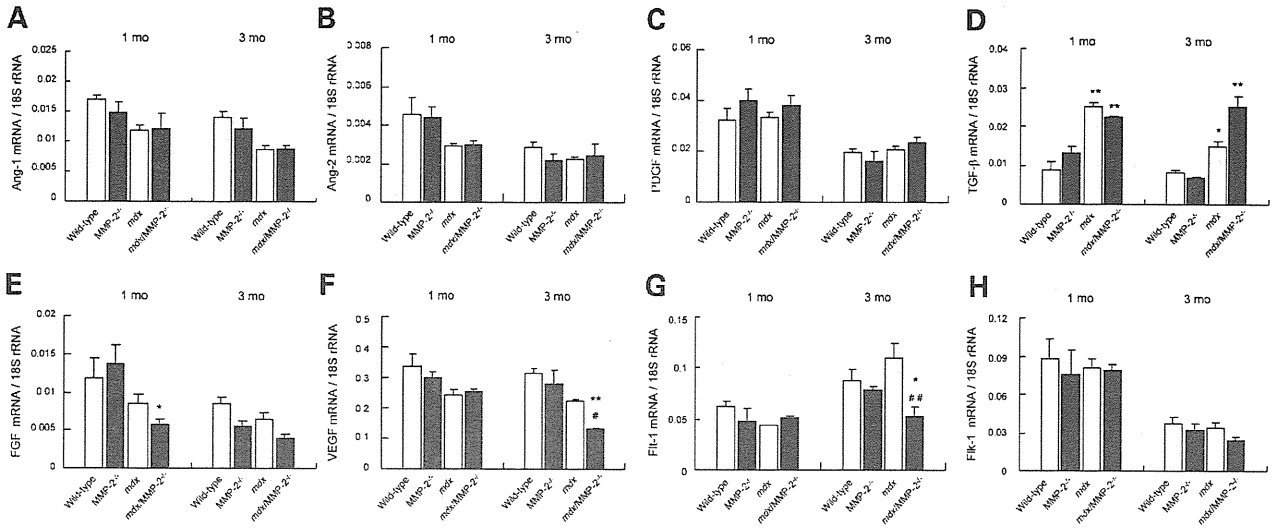

Figure 3. mRNA levels of various angiogenesis-related factors in the *mdx*/MMP-2$^{-/-}$ mice skeletal muscle. Relative (to 18S rRNA) mRNA levels of angiopoietin-1 (**A**), angiopoietin-2 (**B**), PDGF (**C**), FGF (**D**), TGF-β (**E**), VEGF (**F**) and VEGF receptor-1 (Flt-1) (**G**) and -2 (Flk-1) (**H**) in the skeletal muscle of WT, MMP-2$^{-/-}$, *mdx* and *mdx*/MMP-2$^{-/-}$ mice at 1 and 3 months of age ($n = 3$ for each group). Bar: mean ± S.E.M.; $^{*}P < 0.05$, $^{**}P < 0.01$, significantly different from WT; $^{\#}P < 0.05$, $^{\#\#}P < 0.01$, significantly different from MMP-2 ablation alone.

MMP-2 ablation in *mdx* mice down-regulates VEGF

We found that ablation of MMP-2 caused growth impairment of regenerated fibers and of angiogenesis in the *mdx* skeletal muscle at 3 months of age. We hypothesized that the growth impairment might be associated with the abnormality in angiogenesis; therefore, we examined the mRNA levels of various angiogenesis-related factors such as angiopoietin-1 and -2, platelet-derived growth factor (PDGF), fibroblast growth factor (FGF), transforming growth factor-β (TGF-β) and VEGF. No statistical differences in the levels of angiopoietin-1 or -2, PDGF or FGF were detected between *mdx* and *mdx*/MMP-2$^{-/-}$ mice or between WT and MMP-2$^{-/-}$ mice at 1 or 3 months of age (Fig. 3A–C and E). TGF-β mRNA levels were increased in *mdx* and *mdx*/MMP-2$^{-/-}$ mice when compared with WT, but did not significantly change with or without MMP-2 (Fig. 3D). However, we found a significant decrease in the VEGF mRNA level in *mdx*/MMP-2$^{-/-}$ mice when compared with *mdx* mice at 3 months of age (Fig. 3F). We also found a significant decrease in the mRNA level of Flt-1 (VEGF receptor 1), but not Flk-1 (VEGF receptor 2), in *mdx*/MMP-2$^{-/-}$ mice at 3 months of age (Fig. 3G and H). The VEGF protein level was significantly lower in the skeletal muscle of *mdx*/MMP-2$^{-/-}$ mice when compared with *mdx* mice at 3 months of age (Fig. 4A and B). VEGF was localized at neural cell adhesion molecule (NCAM)-positive muscle satellite cells and at the sarcolemma in some muscle fibers (Fig. 4C), but not at Mac-3-positive macrophages (Supplementary Material, Fig. S5). Flt-1 was also localized at most of the NCAM-positive muscle satellite cells. Flk-1-positive cells were identified as vascular endothelial cells by immunoreactivity of PECAM-1 (Fig. 4C). There were no differences in the localizations of VEGF, Flt-1 or Flk-1 between *mdx*/MMP-2$^{-/-}$ and *mdx* mice (Fig. 4C).

It has also been reported that MMP-2 is up-regulated in muscle regeneration in an experimentally injured model (9) and plays a role in myogenesis (17). To determine whether myogenic or growth factors are involved in pathogenesis in *mdx*/MMP-2$^{-/-}$ mice, we investigated the mRNA levels of the myogenic transcription factors Pax-3 and -7, MyoD, Myf5, myogenin and MEF2 in the skeletal muscle. However, there were no statistical differences in the levels of these factors between *mdx* and *mdx*/MMP-2$^{-/-}$ mice or between WT and MMP-2$^{-/-}$ mice at 1 or 3 months of age (Supplementary Material, Fig. S6A–F). There were also no differences in the mRNA levels of the growth factors such as insulin-like growth factor, myostatin or follistatin in the TA muscles between the two groups (Supplementary Material, Fig. S6G–I).

Overexpression of S100 proteins and cytokines in the skeletal muscle of *mdx*/MMP-2$^{-/-}$ mice at 3 months of age

As reported above, we examined the expression levels of various factors related to angiogenesis, myogenesis and growth in the skeletal muscle of *mdx*/MMP-2$^{-/-}$ mice. To determine whether other genes affect pathology in *mdx*/MMP-2$^{-/-}$ mice, we conducted microarrays to comprehensively identify differentially expressed genes in the skeletal muscle of *mdx* and *mdx*/MMP-2$^{-/-}$ mice at 1 and 3 months of age. Based on the profiles of all the genes, we found 113 genes that were differentially (>2- or <0.5-fold) affected by MMP-2 ablation (Supplementary Material, Table S1). Thirteen genes were up-regulated (Supplementary Material, Table S2) and 18 genes were down-regulated (Supplementary Material, Table S3) at 1 month of age, and 69 genes were up-regulated (Supplementary Material, Table S4) and 13 genes were down-regulated (Supplementary Material,

Downloaded from http://hmg.oxfordjournals.org/ at NCNP on May 16, 2012

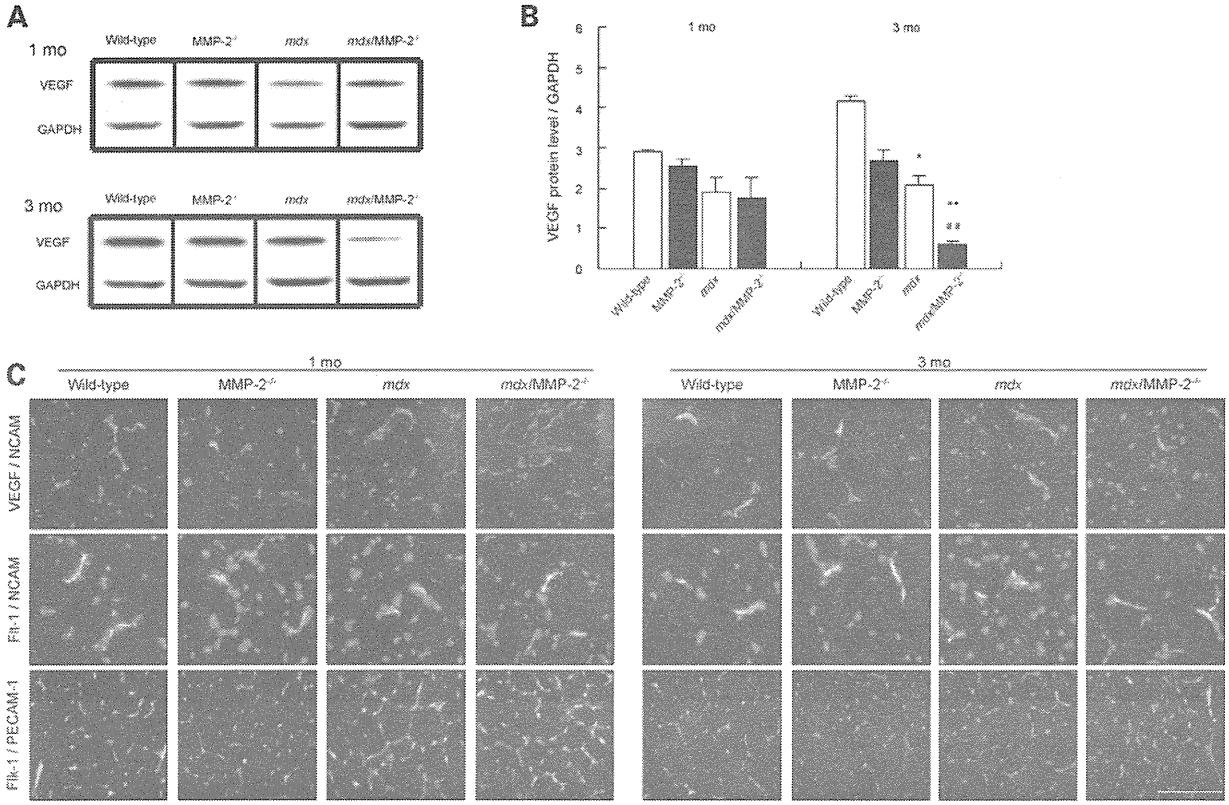

Figure 4. VEGF and its receptor protein levels and localization in the skeletal muscle of *mdx*/MMP-2$^{-/-}$. (A) Western blot analysis of VEGF (upper band) and internal control GAPDH (lower band) in WT, MMP-2$^{-/-}$, *mdx* and *mdx*/MMP-2$^{-/-}$ mice at 1 and 3 months of age. (B) Relative (to GAPDH) VEGF protein levels in WT, MMP-2$^{-/-}$, *mdx* and *mdx*/MMP-2$^{-/-}$ mice at 1 and 3 months of age ($n = 3$ for each group). Bar: mean ± S.E.M.; $^{*}P < 0.05$, $^{**}P < 0.01$, significantly different from WT; $^{\#\#}P < 0.01$, significantly different from MMP-2 ablation alone. (C) Immunohistochemistry of VEGF (red)/NCAM (green) (upper panel), Flt-1 (red)/NCAM (green) (middle panel) and Flk-1 (red)/PECAM-1 (green) (lower panel) in the skeletal muscle of WT, MMP-2$^{-/-}$, *mdx* and *mdx*/MMP-2$^{-/-}$ mice at 1 and 3 months of age. Scale bar: 100 μm.

Table S5) at 3 months of age in *mdx*/MMP-2$^{-/-}$ mice when compared with *mdx* mice (Supplementary Material, Fig. S7A and B). The genes that were up-regulated at 3 months of age in *mdx*/MMP-2$^{-/-}$ mice were mainly involved with protein binding, cytokine and its receptor or cell growth. Among the genes up-regulated at 3 months of age, S100 calcium-binding protein A8 (S100A8) and A9 (S100A9), cytokines such as chemokine C-C motif ligand (CCL)-2 and-7, chemokine C-C motif receptor (CCR)-1 and -2, and chitinase 3-like 3 were highly up-regulated in *mdx*/MMP-2$^{-/-}$ mice (Supplementary Material, Table S4). We confirmed these results by using quantitative real-time polymerase chain reaction (RT-PCR; Supplementary Material, Fig. S7C–I).

MMP-2 ablation further decreases nNOS expression in the skeletal muscle of *mdx* mice

Nitric oxide (NO) is a vasodilator produced by nitric oxide synthase (NOS), and inhibition of NOS activity abolishes capillary proliferation in electrically stimulated skeletal muscles (25). In electrically stimulated skeletal muscles, expression of endothelial NOS (eNOS) and nNOS increase in the early and late stages of angiogenesis, respectively (25–27). nNOS is linked to DGC, and dystrophin deficiency causes a reduction in nNOS expression at the sarcolemma, resulting in modification of dystrophic pathology (28,29). Thus, we examined the mRNA levels of nNOS, eNOS and inducible NOS (iNOS) produced by invaded inflammatory cells in the skeletal muscle of *mdx*/MMP-2$^{-/-}$ mice. mRNA expression of nNOS, but not of eNOS and iNOS, was significantly lower in *mdx*/MMP-2$^{-/-}$ than in *mdx* mice at 3 months of age (Fig. 5A–C). Western blotting also revealed that the nNOS protein level was significantly lower in *mdx*/MMP-2$^{-/-}$ than in *mdx* mice at 3 months of age (Fig. 5D and E), although there were no apparent differences in nNOS immunoreactivity between the *mdx*/MMP-2$^{-/-}$ and *mdx* mice (Fig. 5F). These results suggest that down-regulation of nNOS in the regenerated skeletal muscle of *mdx*/MMP-2$^{-/-}$ mice may influence impairment of angiogenesis.

MMP-2 does not affect the degradation of DGC components in the process of dystrophic muscle regeneration

DGs comprise two subunits, a highly glycosylated ECM protein, α-dystroglycan (α-DG), and a transmembrane

Downloaded from http://hmg.oxfordjournals.org/ at NCNP on May 16, 2012

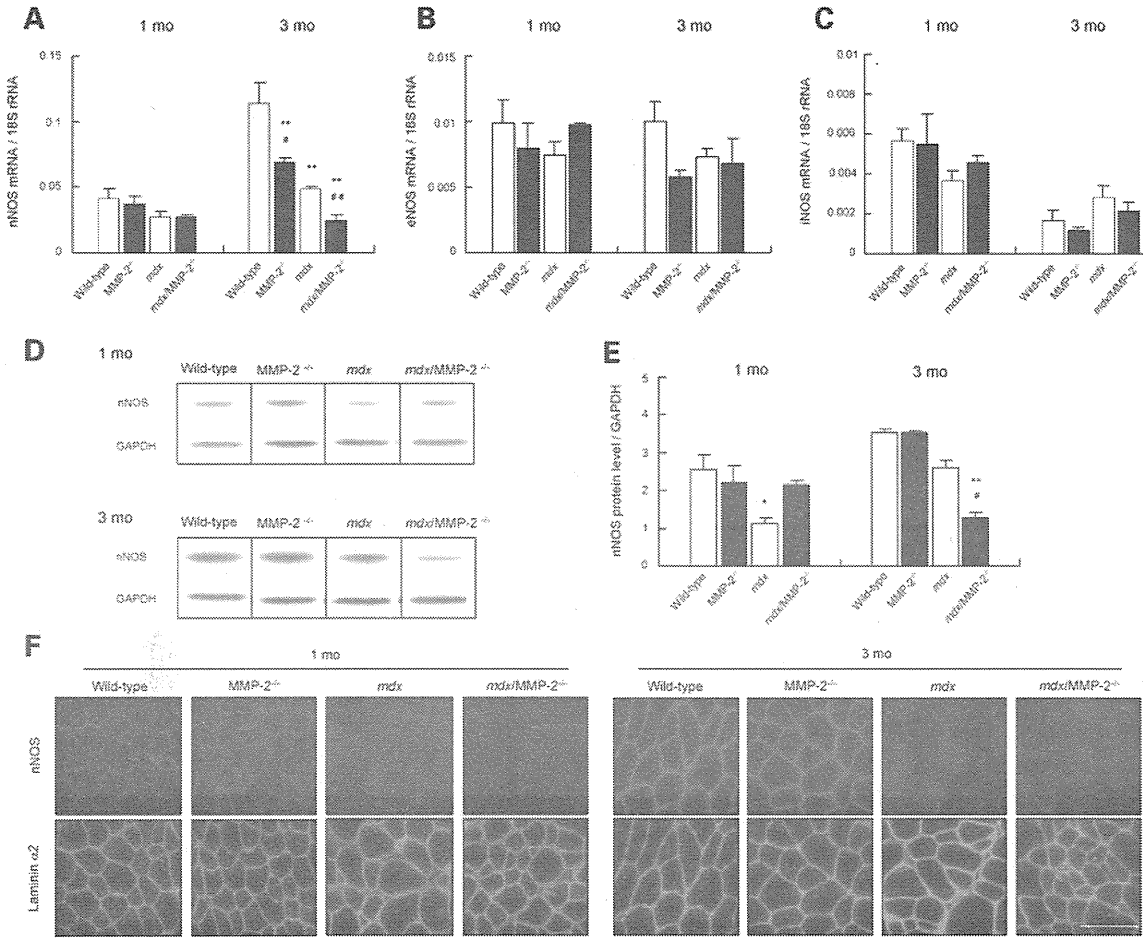

Figure 5. NOS isoform expression in the skeletal muscle of *mdx*/MMP-$2^{-/-}$ mice. Relative (to 18S rRNA) mRNA levels of nNOS (**A**), eNOS (**B**) and iNOS (**C**) in the skeletal muscle of WT, MMP-$2^{-/-}$, *mdx* and *mdx*/MMP-$2^{-/-}$ mice ($n = 3$ for each group). Bar: mean ± S.E.M.; $^{**}P < 0.01$, significantly different from WT; $^{\#}P < 0.05$, $^{\#\#}P < 0.01$, significantly different from MMP-2 ablation alone. (**D**) Western blot analysis of nNOS and (**E**) relative (to GAPDH) nNOS protein levels in the skeletal muscle of WT, MMP-$2^{-/-}$, *mdx* and *mdx*/MMP-$2^{-/-}$ mice ($n = 3$ for each group). Bar: mean ± S.E.M.; $^{*}P < 0.05$, $^{**}P < 0.01$, significantly different from WT; $^{\#}P < 0.05$, significantly different from MMP-2 ablation alone. (**F**) Immunohistochemistry of nNOS and laminin α2 in the skeletal muscle of WT, MMP-$2^{-/-}$, *mdx* and *mdx*/MMP-$2^{-/-}$ mice. Scale bar: 100 μm.

protein, β -dystroglycan (β-DG). DGs are membrane receptors involved with the complex of glycoproteins associated with dystrophin (30), and their interaction is crucial in maintaining the integrity of the plasma membrane. In the dystrophin-deficient muscle, the interaction between the two DG subunits may be disrupted by the proteolytic activity of MMPs (12). Previous research has examined the proteolytic activities of human MMP-9 and MMP-2 on the recombinant extracellular domain of β-DG and characterized a cleavage site by MMP-9 on β-DG (31). However, the molecular mechanism underlying the effect of MMP-2 is still unknown. We examined whether MMP-2 ablation in *mdx* mice affects processing of DGC in the skeletal muscle. In the skeletal muscle of both *mdx* and *mdx*/MMP-$2^{-/-}$ mice at 1 and 3 months of age, full-length 43-kDa β-DG (βDG_{43}) was cleaved to a 30-kDa form of β-DG (βDG_{30}) (Fig. 6A); however, although the degree of degradation in *mdx*/MMP-$2^{-/-}$ mice was less than that in *mdx* mice at 1 month of age, it was not different at 3 months of age (Fig. 6B and C). Similarly, expression of β-sarcoglycan did not change in the skeletal muscle of *mdx*/MMP-$2^{-/-}$ mice at 1 or 3 months of age when compared with *mdx* of the same age (Supplementary Material, Fig. S8). In the process of regeneration of the dystrophic muscle, MMP-2 may not have a critical role in the degradation of DGC components.

DISCUSSION

In this study, we investigated the role of MMP-2 in the dystrophic skeletal muscle using *mdx* mice with MMP-2 ablation (*mdx*/MMP-$2^{-/-}$). The histopathology of the skeletal muscle in *mdx*/MMP-$2^{-/-}$ mice at 3 months of age showed small regenerated muscle fibers and an impairment of angiogenesis when compared with *mdx* mice at the same age. The impaired growth of regenerating muscle fibers was also observed in the

Downloaded from http://hmg.oxfordjournals.org/ at NCNP on May 16, 2012

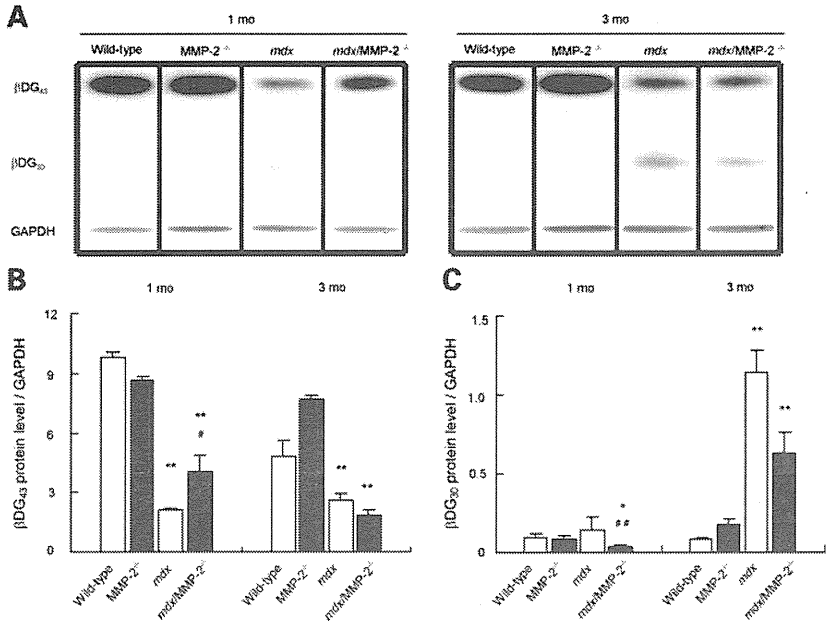

Figure 6. β-DG degradation in the *mdx*/MMP-2$^{-/-}$ mice skeletal muscle. (**A**) Western blot analyses of β-DG in the skeletal muscle of WT, MMP-2$^{-/-}$, *mdx* and *mdx*/MMP-2$^{-/-}$ mice. Full-length β-DG (βDG_{43}, upper bands) and degraded 30-kDa proteins (βDG_{30}, lower bands) were observed in both *mdx* or *mdx*/MMP-2$^{-/-}$ mice at 1 and 3 months of age. Relative (to GAPDH) levels of βDG_{43} (**B**) and βDG_{30} (**C**) revealed an increase in βDG_{43} and a decrease in βDG_{30} in *mdx*/MMP-2$^{-/-}$ when compared with *mdx* at 1 month of age. Bar: mean ± S.E.M.; $^{*}P < 0.05$, $^{**}P < 0.01$, significantly different from WT; $^{\#}P < 0.05$, $^{\#\#}P < 0.01$, significantly different from MMP-2 ablation alone.

cardiotoxin injury model of MMP-2$^{-/-}$ mice, suggesting that MMP-2 may play an important role in the muscle regeneration under certain disease conditions. MMP-2, a primary MMP derived from vascular endothelial cells and smooth muscle cells, degrades various ECM proteins (32,33) and is implicated as a key player in vascular development and angiogenesis (34). MMP-2 knockout mice have demonstrated a reduction in angiogenesis and corresponding tumor growth (24) and impairment of ischemia-induced neovascularization through a decreased number of endothelial cells and endothelial progenitor cells (16). Therefore, we hypothesized that the close relationship between impairment of regenerated myofiber growth and reduction in angiogenesis in the *mdx*/MMP-2$^{-/-}$ mice might allow us to identify factors related to angiogenesis or growth in these mice. We subsequently found a reduction of VEGF expression in the regenerated skeletal muscle of the mice at 3 months of age.

VEGF plays an important role in mediating both physiological and pathological angiogenesis via inducing vasodilation or vascular permeability, and by stimulating the proliferation, migration and survival of endothelial cells (35). In a previous study, both cultured satellite cells and myoblasts expressed VEGF and VEGFR-1 and -2; furthermore, administration *in vitro* stimulates myoblast migration and survival, protects myogenic cells from apoptosis and promotes myogenic cell growth (36). In normal muscles, VEGF and its receptors are expressed in vascular structures and not in muscle fibers; however, they are expressed in satellite cells and regenerating muscle fibers after experimental muscle damage, suggesting the operation of an autocrine pathway that may promote the survival and regeneration of myocytes (37). This study also demonstrates that the introduction of VEGF by using a virus vector promotes regeneration via angiogenesis, resulting in the decrease in muscle damage as well as the promotion of muscle regeneration and function in *mdx* mice (37). Meanwhile, another study shows that VEGF administration by using viral vectors injected in the normal mouse skeletal muscle results in the appearance of a notable subset of muscle fibers exhibiting muscle regeneration. Moreover, the delivery of VEGF markedly promotes muscle fiber regeneration with a dose-dependent effect after experimental muscle damage with ischemia, glycerol or cardiotoxin (38). Furthermore, the increased density of satellite cells has been observed adjacent to capillaries, suggesting a possible role of VEGF in homing circulating progenitor germ cells to specific muscle location and/or in regulating the satellite cells pool (39). Taken together, VEGF might function during regeneration not only through neovascularization, but also by directly acting on muscle cells and on the recruitment of progenitor cells from bone marrow during dystrophic pathology. VEGF was down-regulated in an ischemic-induced model using MMP-2 knockout mice due to a reduction in the number of invasive macrophages producing VEGF (16). However, our data indicate that VEGF is localized in NCAM-positive satellite cells and the sarcolemma in certain muscle fibers (Fig. 4C), but not in Mac-3-positive macrophages (Supplementary Material, Fig. S5). In a recent report, MMP-2 transcriptional inactivation by using an siRNA-based approach both in *in vitro* and *in vivo* significantly reduced integrin-αVβ3-mediated phosphoinositide 3-kinase/AKT-induced VEGF expression, which ultimately decreased tumor cell-induced angiogenesis (40). Similar mechanism might also underlie the relationship between MMP-2 and VEGF in the

Downloaded from http://hmg.oxfordjournals.org/ at NCNP on May 16, 2012

dystrophic muscle. Although VEGF is known to be located upstream of MMP-2, we suggest that MMP-2 and VEGF may regulate each other in the skeletal muscle.

We conducted microarrays to comprehensively identify differentially expressed genes in *mdx*/MMP-2$^{-/-}$ mice, because other genes could affect the phenotype. Among the genes up-regulated at 3 months of age in *mdx*/MMP-2$^{-/-}$ mice, S100A8 and A9 mRNA levels were significantly increased. S100 proteins are involved in the pathogenesis of cellular stress condition such as wound healing or inflammatory disorders (41). In particular, S100A8 and A9 are required for transcriptional activation of the *MMP-2* gene (42). We suggest, therefore, that overexpression of S100A8 and A9 in *mdx*/MMP-2$^{-/-}$ mice may compensate for MMP-2 ablation. In addition, microarray analysis (Supplementary Material, Table S4) and RT-PCR revealed that MMP-3 was significantly increased in the skeletal muscle of *mdx*/MMP-2$^{-/-}$ mice at 3 months of age when compared with that of the age-matched *mdx* mice. It has been reported that MMP-3 is significantly elevated in the synovium by intra-articular injection of recombinant S100A8 in knee joints of normal mice and was increased in macrophages stimulated by recombinant S100A8 or S100A8/A9 heterodimer (43). The up-regulation of MMP-3 in the skeletal muscle of *mdx*/MMP-2$^{-/-}$ mice at 3 months of age may be caused by overexpression of S100A8 and A9.

We also found that expression of nNOS in the *mdx*/MMP-2$^{-/-}$ mice was significantly lower than in *mdx* mice at 3 months of age. This further reduction in nNOS may have been caused by MMP-2 ablation in the *mdx* mice, or impairment of angiogenesis may secondarily induce a further decrease in nNOS. NO is increased in the ischemic hindlimb and eliminating NO impairs the revascularization process (44). It has been reported that an nNOS transgene in *mdx* mice ameliorated muscular dystrophy (45) and that *mdx* mice expressed dystrophin only in smooth muscle cells, restoring vascular nNOS expression and NO-dependent vasoregulation and resulting in improvement in dystrophic pathology (46). Taken together, these studies show that MMP-2 ablation in *mdx* mice may result in further reduction of nNOS in the dystrophic muscle, with a detrimental effect on the function and regeneration of the dystrophic muscle. It is reported that nNOS levels are reduced in inflammatory conditions (47). Actually, our data showed that the expression of some cytokines (e.g. CCL-2) was significantly increased in the skeletal muscle of *mdx*/MMP-2$^{-/-}$ at 3 months of age. Taken a report that S100A8/A9 enhances the gene expression of pro-inflammatory proteins such as CCL-2 (48), S100A8/A9 up-regulation may enhance pro-inflammatory genes, resulting in the down-regulation of nNOS expression in *mdx*/MMP-2$^{-/-}$ mice at 3 months of age. Interestingly, nNOS$^{-/-}$ mice in an acute lung injury model show reduced expression of VEGF protein (49). The decrease in nNOS levels via increased cytokines may also reduce VEGF expression in the skeletal muscle of *mdx*/MMP-2$^{-/-}$ mice at 3 months of age.

We assessed differences in the degradation patterns of DGC in the skeletal muscles between *mdx* and *mdx*/MMP-2$^{-/-}$ mice. The β-DG degradation was reduced by MMP-2 ablation in *mdx* mice at 1 month of age. Nevertheless, at 3 months of age, β-DG degradation was unchanged in the presence of MMP-2. Previous reports documented that MMP-2 as well as MMP-9 were able to degrade β-DG (50) and that macrophage-derived MMP-2 in a mouse model of experimental autoimmune encephalomyelitis participated in tissue injury via β-DG degradation through proteolytic activity (10). However, our data indicated that β-DG degradation by MMP-2 was not apparent in the process of muscle regeneration. The expression of β-sarcoglycan remained unchanged in the skeletal muscle of *mdx*/MMP-2$^{-/-}$ mice at 1 and 3 months of age when compared with *mdx* of the same age. These results suggest that the ablation of MMP-2 does not significantly influence the degradation of β-DG and β-sarcoglycan in the regeneration process of the dystrophic muscle.

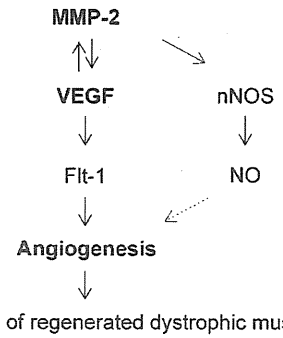

Figure 7. Hypothetical schema of the role of MMP-2 in the dystrophin-deficient skeletal muscle. We hypothesize that MMP-2 influences angiogenesis and muscle regeneration via up-regulation of VEGF and its receptor Flt-1 during regeneration of the dystrophin-deficient skeletal muscle. MMP-2 may also affect angiogenesis in the dystrophin-deficient skeletal muscle through coordination of NO produced by nNOS.

In this study, we found that reduction in angiogenesis via decreased VEGF and nNOS expression may impair regeneration in the skeletal muscle of *mdx* mice with MMP-2 ablation (Fig. 7). Corticosteroids are promising agents for the prevention of progression in various diseases including DMD; however, they inhibit VEGF and MMP-2, resulting in a reduction in tissue angiogenesis (51,52). Normal rats treated with corticosteroids exhibit muscle atrophy and weakness with a concomitant reduction in VEGF expression (53,54); therefore, the decrease in MMP-2 and VEGF by corticosteroids might be associated with the pathogenesis in steroid myopathy.

MATERIALS AND METHODS

Mice

Control (strain: C57 BL/6J) and MMP-2 knockout (strain: C57BL/6J-Mmp2tm) mice were purchased from Jackson Laboratory (Bar Harbor, ME, USA). Dystrophin-deficient (*mdx*) mice (strain: C57BL/6J-DMD*mdx*) were a gift from the Institute of Neuroscience, National Research Center of Neurology and Psychiatry (Tokyo, Japan). MMP-2 knockout (MMP-2$^{-/-}$) mice were crossed with *mdx* mice to generate littermate WT, MMP-2$^{-/-}$, *mdx*/MMP-2$^{+/+}$ and *mdx*/MMP-2$^{-/-}$ mice. All genotypes were determined using PCR

Downloaded from http://hmg.oxfordjournals.org/ at NCNP on May 16, 2012

analysis of mice tail DNA. An amplification-resistant mutation system assay was used to identify control and *mdx* mice (55). MMP-2 knockout and control mice were identified using the primer sets suggested by the Jackson Laboratory. Mice were housed in a plastic cage in a temperature-controlled environment with a 12-h light/dark cycle and free access to food and water. All experiments with animals were carried out in accordance with the institutional guidelines and approved by the Institutional Review Board of Shinshu University, Japan.

Muscle tissue extraction and preparation

TA muscles were carefully dissected and frozen in isopentane cooled by liquid nitrogen for histological and immunohistochemical analyses and protein and RNA isolation, and were stored at −80°C. Ten-micrometer transverse cryostat sections were cut in the center of the TA muscle belly to obtain the largest cross-sectional area (CSA), placed on slides, air-dried and stained with hematoxylin and eosin (H&E). Serial sections were stained to demonstrate myofibrillar ATPase activity. Diaphragm, quadriceps and gastrocnemius muscles were also dissected and frozen, and were stained with H&E as noted above. The sections were viewed and photographed using a digital camera system (Leica Microsystems, Wetzlar, Germany).

Cardiotoxin muscle injury and histochemistry

We injected 100 μl of cardiotoxin (10 mM in 0.9% NaCl) (Sigma, St Louis, MO, USA) into the TA muscle of WT and MMP-2$^{-/-}$ mice at 6 weeks of age using a 27-gage needle and a 1-ml syringe. The needle was inserted deep into the TA muscle longitudinally toward the knee from the ankle. The needle was held in place for a few seconds and then slowly withdrawn along the long axis of the anterior tibial muscle with a little pressure to allow the cardiotoxin to permeate throughout the muscle. The TA muscles were isolated before the injection, and 3 and 7 days after; the muscles were then frozen in liquid nitrogen-cooled isopentane. Ten-micrometer transverse cryostat sections were stained with H&E, and the diameters of 500 muscle fibers were measured.

Morphometric analysis

Morphometric analysis was performed to determine the CSA of each muscle fiber by using the H&E-stained TA, diaphragm, quadriceps and gastrocnemius muscle sections, separately recording the CSAs for perinuclear fibers and centronuclear regenerated fibers. Necrotic fibers, when present, were discarded. The distribution of muscle fiber CSAs was examined using National Institutes of Health (Bethesda, MD, USA) images. At least 1000 fibers were analyzed for each muscle, and muscle fiber boundaries were determined to count the size and number of the fibers. All images were obtained under identical conditions and at the same magnification. For the CSA histogram, histological parameters were evaluated and treated as previously described (56). Variability in fiber size was determined by the mean ± S.E.M. values.

Study for vessels was performed on 6-μm-thick TA muscle sections stained with anti-PECAM-1 antibody. Serial H&E-stained sections were used to count the number of muscle fibers. The number and size of each vessel and number of muscle fibers were counted under identical conditions and at same magnification. We determined the number of vessels per myofiber and endothelial area of PECAM-1-positive vessels in total area.

Immunohistochemical analysis

For immunofluorescent staining, serial cross-sections (6-μm thick) from frozen skeletal muscle tissues were mounted on glass slides. The sections were air-dried and blocked in 10% goat serum in phosphate-buffered saline (PBS) for 30 min and incubated with primary antibodies in blocking solution at 4°C overnight. The sections were washed briefly with 1× PBS before incubation with secondary antibodies for 1 h at room temperature and then washed three times for 30 min with 1× PBS. The slides were mounted using a fluorescence medium with 4′,6-diamidino-2-phenylindole (Vector Laboratories, Burlingame, CA, USA), visualized using a fluorescent microscope (Olympus, Tokyo, Japan), and images were captured using a VB-7010 camera (Keyence, Osaka, Japan). The primary antibody dilutions and sources were as follows: rat monoclonal anti-PECAM-1 (1:50; BD Transduction Laboratories, San Jose, CA, USA), rabbit polyclonal anti-VEGF-A (1:50; Santa Cruz Biotechnology, Santa Cruz, CA, USA), rabbit polyclonal anti-Flt-1 (1:100; Santa Cruz Biotechnology), rabbit monoclonal anti-Flk-1 (1:100; Cell Signaling Technology, Danvers, MA, USA), rat monoclonal anti-laminin α2-chain (1:100; Enzo Life Sciences, Plymouth Meeting, PA, USA), rabbit polyclonal anti-nNOS (1:200; Invitrogen, Carlsbad, CA, USA), rat monoclonal anti-NCAM (1:100; Millipore, Billerica, MA, USA), rat monoclonal anti-Mac3 (1:50 BD; Transduction Laboratories), mouse anti-β-sarcoglycan (1:200; Leica Microsystems). Alexa Fluor® 488 or Alexa Fluor® 568-conjugated secondary antibodies were obtained from Invitrogen and used at 1:500 dilution.

Total protein extract and western blotting

Muscle tissues (20 mg) were homogenized in 150 μl of 5% sodium dodecyl sulfate (SDS) sample buffer (50 μmol/l Tris–HCl, pH 8.0, 10 μmol/l ethylenediaminetetraacetic acid, 5% SDS and 5% β-mercaptoethanol). After centrifugation (10 min at 15 000*g*), the protein concentration was estimated in the supernatant using the BCA Protein Assay Kit (Bio-Rad, Hercules, CA, USA). Protein homogenates recovered from the supernatant from each sample were denatured for 5 min at 95°C in reducing buffer (50 μl of SDS buffer containing 5% SDS, 0.01% bromophenol blue, 10% glycerol and 5% β-mercaptoethanol). Protein extracts (10 μg/lane) were submitted to SDS-polyacrylamide gel electrophoresis (7.5 or 12.5%) with pre-stained standard proteins (Bio-Rad) to achieve more accurate molecular weight determination. The resulting gel was transferred onto a 0.2-μm nitrocellulose membrane (Millipore) using a transfer buffer (25 mmol/l Tris–HCl, pH 8.3, 192 mmol/l glycine and 20% methanol). The membranes were blocked with Tris buffer, 0.1% Tween 20 (TBST) containing 5% milk (w/v) for 1 h at room

Downloaded from http://hmg.oxfordjournals.org/ at NCNP on May 16, 2012

temperature. All membranes were incubated with primary antibodies at 4°C overnight followed by several washes with TBST. The membranes were incubated with peroxidase-conjugated secondary antibodies (Bio-Rad) for 1 h, washed several times with the washing buffer described above and visualized using an enhanced chemiluminescence system according to the manufacturer's protocol (Amersham, Little Chalfont, UK). Protein signals were quantified by scanning densitometry using the program package of the National Institutes of Health. The results from each experimental group were expressed as integrated intensities relative to the control samples. Equal loading of proteins was assessed on stripped blots by immunodetection using the anti-glyceraldehyde-3-phosphate dehydrogenase (GAPDH) antibody. The primary antibody dilutions and sources were as follows: goat anti-VEGF-A (1:200; Santa Cruz Biotechnology), mouse anti-nNOS (1:1000; BD Transduction Laboratories), rabbit anti-MMP-9 (1:1000; Millipore), mouse anti-β-DG (1:800; Leica Microsystems), mouse anti-β-sarcoglycan (1:400; Leica Microsystems) and mouse anti-GAPDH (1:3000; Millipore).

Gelatin zymography

Frozen skeletal muscles were homogenized in an extraction buffer (62.5 mM Tris–HCl, pH 6.8, 2% SDS and 10% glycerol), and total protein content was assessed using a BCA Protein Assay Kit (Bio-Rad). Each extract (50 μg) was dissolved in a loading buffer provided by the manufacturer and subsequently electrophoresed through a gelatin-containing SDS-polyacrylamide gel provided as part of the Gelatin Zymography Kit (Invitrogen). The gel was washed with regenerating buffer and subsequently incubated for 24 h at 37°C in developing buffer that was also provided by the manufacturer. The gels were stained in Coomasie Brilliant Blue (CBB) and destained with a destaining solution (Bio-Rad). Gelatinolytic activity was identified as clear bands on a blue background. Gelatin zymography detects the activity of both pro- and active forms of gelatinolytic MMPs. This is because exposure to SDS during gel electrophoresis activates the pro-form MMPs without proteolytic cleavage of the prodomain. Equality of the protein concentration was confirmed by CBB staining. Myosin heavy chain was used as a loading control.

RNA isolation and gene expression profiling

Frozen tissues (20 mg) for each muscle were homogenized, and the total RNA was isolated using an RNeasy Fibrous Tissue Kit (Qiagen, Hilden, Germany) according to the manufacturer's instructions. cDNA synthesis, biotin-labeled target synthesis, Mouse Genome 430 2.0 Array Gene Chip (Affymetrix, Santa Clara, CA, USA) array hybridization, staining and scanning were performed according to the standard protocols supplied by Affymetrix. The quality of the data was controlled using Microarray Suite MAS 5.0 (Affymetrix). The MAS-generated raw data were uploaded to GeneSpring GX software version 10 (Silicon Genetics, Redwood City, CA, USA). The software calculated signal intensities, and each signal was normalized to the median of its values in all samples or the 50th percentile of all signals for a specific hybridization experiment. Fold ratios were obtained by comparing normalized data for *mdx* and *mdx*/MMP-$2^{-/-}$ mice.

Analyses by RT-PCR

Single-strand cDNA was synthesized using the QuantiTect Reverse Transcription Kit (Qiagen). The levels of mRNA and 18S rRNA were quantified using fluorescent dye SYBR-green detection (Roche Diagnostics, Basel, Switzerland) with 10 nM of each primer at a final volume of 10 μl, and the reactions were carried out in duplicate using the StepOnePlus RT-PCR system (Applied Biosystems, Foster City, CA, USA). Thermal cycling conditions for all primers were 10 min at 95°C, then 40 cycles each of 15 s at 94°C, 30 s at 48°C, 1 min at 72°C and a final extension of 10 min at 72°C. For each gene, all samples were amplified simultaneously. Each RNA quantity was normalized to its respective 18S rRNA mRNA quantity. Primer sequences for RT-PCR are shown in Supplementary Material, Table S1.

Statistical analysis

Results are expressed as mean ± S.E.M. Statistical analysis was performed using an unpaired *t*-test for two-group comparisons, and multiple comparisons were performed using a one-way ANOVA. Intergroup comparison was carried out using the Bonferroni correction. Statistical significance was set at $P < 0.05$. Statistical analyses were carried out using the software SigmaStat, version 2.0 (Aspire Software, Ashburn, VA, USA).

SUPPLEMENTARY MATERIAL

Supplementary Material is available at *HMG* online.

Conflict of Interest statement. None declared.

FUNDING

This work was supported by Grants-in-Aid for Scientific Research (B) from the Ministry of Education, Culture, Sports, Science and Technology of Japan (21300157 to A.N.).

REFERENCES

1. Emery, A.E. and Gosden, C. (1974) A neurogenic component in muscular dystrophy. *J. Med. Genet.*, **11**, 76–79.
2. Hoffmann, E.P., Monaco, A.P., Feener, C.C. and Kunkel, L.M. (1987) Conservation of the Duchenne muscular dystrophy gene in mice and humans. *Science*, **238**, 347–350.
3. Ervasti, J.M. and Campbell, K.P. (1991) Membrane organization of the dystrophin–glycoprotein complex. *Cell*, **66**, 1121–1131.
4. Ibraghimov-Beskrovnaya, O., Ervasti, M.J., Leveille, J.C., Slaughter, A.C., Sernett, W.S. and Campbell, P.K. (1992) Primary structure of dystrophin-associated glycoproteins linking dystrophin to the extracellular matrix. *Nature*, **355**, 696–702.
5. Allen, D.G., Whitehead, N.P. and Yeung, E.W. (2005) Mechanisms of stretch-induced muscle damage in normal and dystrophic muscle: role of ionic changes. *J. Physiol.*, **567**, 723–735.
6. Mott, J.D. and Werb, Z. (2004) Regulation of matrix biology by matrix metalloproteinases. *Curr. Opin. Cell Biol.*, **16**, 558–564.
7. Vu, T.H. and Werb, Z. (2000) Matrix metalloproteinases: effectors of development and normal physiology. *Genes Dev.*, **14**, 2123–2133.
8. Nagase, H. and Woessner, J.F. Jr (1999) Matrix metalloproteinases. *J. Biol. Chem.*, **274**, 21491–21494.

Downloaded from http://hmg.oxfordjournals.org/ at NCNP on May 16, 2012

9. Kherif, S., Lafuma, C., Dehaupas, M., Lachkar, S., Fournier, J.G., Verdiere-Sahuque, M., Fardeau, M. and Alameddine, H.S. (1999) Expression of matrix metalloproteinase 2 and 9 in regenerating skeletal muscle: a study in experimentally injured and *mdx* muscles. *Dev. Biol.*, **205**, 158–170.
10. Agrawal, S., Anderson, P., Durbeej, M., Rooijen, N., Ivars, F., Opdenakker, G. and Sorokin, L.M. (2006) Dystroglycan is selectively cleaved at the parenchymal basement membrane at sites of leukocyte extravasation in experimental autoimmune encephalomyelitis. *J. Exp. Med.*, **203**, 1007–1019.
11. Zhong, D., Saito, F., Saito, Y., Nakamura, A., Shimizu, T. and Matsumura, K. (2006) Characterization of the protease activity that cleaves the extracellular domain of β-dystroglycan. *Biochem. Biophys. Res. Commun.*, **345**, 867–871.
12. Matsumura, K., Zhong, D., Saito, F., Arai, K., Adachi, K., Kawai, H., Higuchi, I., Nishino, I. and Shimizu, T. (2005) Proteolysis of β-dystroglycan in muscular disease. *Neuromuscul. Disord.*, **15**, 336–341.
13. Nakamura, A., Yoshida, K., Ueda, H., Takeda, S. and Ikeda, S. (2005) Up-regulation of mitogen activated protein kinases in *mdx* skeletal muscle following chronic treadmill exercise. *Biochim. Biophys. Acta*, **1740**, 326–331.
14. Fukushima, K., Nakamura, A., Ueda, H., Yuasa, K., Yoshida, K., Takeda, S. and Ikeda, S. (2007) Activation and localization of matrix metalloproteinase-2 and -9 in the skeletal muscle of the muscular dystrophy dog ($CXMD_J$). *BMC Musculoskelet. Disord.*, **8**, 1–11.
15. Li, H., Mittal, A., Makonchuk, D.Y., Bhatnagar, S. and Kumar, A. (2009) Matrix metalloproteinase-9 inhibition ameliorates pathogenesis and improves skeletal muscle regeneration in muscular dystrophy. *Hum. Mol. Genet.*, **18**, 2584–2598.
16. Chen, X.W., Kuzuya, M., Nakamura, K., Maeda, K., Tsuzuki, M., Kim, W., Sasaki, T., Liu, Z., Inoue, N., Kondo, T. *et al.* (2007) Mechanisms underlying the impairment of ischemia-induced neovascularization in matrix metalloproteinase 2-deficient mice. *Circ. Res.*, **100**, 904–913.
17. Lluri, G. and Jaworski, E.M. (2005) Regulation of TIMP-2, MT1-MMP, and MMP-2 expression during C2C12 differentiation. *Muscle Nerve*, **32**, 492–499.
18. Zimowska, M., Brzoska, E., Swierczynska, M., Streminska, W. and Moraczewski, J. (2008) Distinct patterns of MMP-9 and MMP-2 activity in slow and fast twitch skeletal muscle regeneration *in vivo*. *Int. J. Dev. Biol.*, **52**, 307–314.
19. Itoh, T., Ikeda, T., Gomi, H., Nakao, S., Suzuki, T. and Itohara, S. (1997) Unaltered secretion of β-amyloid precursor protein in gelatinase A (matrix metalloproteinase 2)-deficient mice. *J. Biol. Chem.*, **272**, 22389–22392.
20. Fähling, M., Steege, A., Perlewitz, A., Nafz, B., Mrowka, R., Persson, P.B. and Thiele, B.J. (2005) Role of nucleolin in posttranscriptional control of MMP-9 expression. *Biochim. Biophys. Acta*, **1731**, 32–40.
21. Gillis, J.M. (1999) Understanding dystrophinopathies: an inventory of the structural and functional consequence of the absence of dystrophin in muscles of the *mdx* mouse. *J. Muscle Res. Cell Motil.*, **20**, 605–625.
22. Collen, A., Hanemaaijer, R., Lupu, F., Quax, P.H., van Lent, N., Grimbergen, J., Peters, E., Koolwijk, P. and Hinsbergh, V.W. (2003) Membrane-type matrix metalloproteinase-mediated angiogenesis in a fibrin-collagen matrix. *Blood*, **101**, 1810–1817.
23. Silletti, S., Kessler, T., Goldberg, J., Boger, D.L. and Cheresh, D.A. (2001) Disruption of matrix metalloproteinase 2 binding to integrin alpha v beta 3 by an organic molecule inhibits angiogenesis and tumor growth *in vivo*. *Proc. Natl Acad. Sci. USA*, **98**, 119–124.
24. Itoh, T., Tanioka, M., Yoshida, H., Yoshioka, T., Nishimoto, H. and Itohara, S. (1998) Reduced angiogenesis and tumor progression in gelatinase A-deficient mice. *Cancer Res.*, **58**, 1048–1051.
25. Milkiewicz, M., Hudlicka, O., Brown, M.D. and Silgram, H. (2005) Nitric oxide, VEGF and VEGFR-2: interactions in activity-induced angiogenesis in rat skeletal muscle. *Am. J. Physiol.*, **289**, H336–H343.
26. Reiser, P.J., Kline, W. and Vaghy, P.L. (1997) Induction of neuronal type nitric oxide synthase in skeletal muscle by chronic electrical stimulation *in vivo*. *J. Appl. Physiol.*, **83**, 1250–1255.
27. Hudlicka, O. and Brown, M.D. (2009) Adaptation of skeletal muscle microvasculature to increased or decreased blood flow: role of shear stress, nitric oxide and vascular endothelial growth factor. *J. Vasc. Res.*, **46**, 504–512.
28. Brenman, J.E., Chao, D.S., Xia, H., Aldape, K. and Bredt, D.S. (1995) Nitric oxide synthase complexed with dystrophin and absent from skeletal muscle sarcolemma in Duchenne muscular dystrophy. *Cell*, **82**, 743–752.
29. Chang, W.J., Iannaccone, S.T., Lau, K.S., Masters, B.S.S., McCabe, T.J., McMillan, K., Padre, R.C., Spencer, M.J., Tidball, J.G. and Stull, J.T. (1996) Neuronal nitric oxide synthase and dystrophin-deficient muscular dystrophy. *Proc. Natl Acad. Sci. USA*, **93**, 9142–9147.
30. Yamada, H., Saito, F., Fukuta-Ohi, H., Zhong, D., Hase, A., Arai, K., Okuyama, A., Maekawa, R., Shimizu, T. and Matsumura, K. (2001) Processing of β-dystroglycan by matrix metalloproteinase disrupts the link between the extracellular matrix and cell membrane via the dystroglycan complex. *Hum. Mol. Genet.*, **10**, 1563–1569.
31. Bozzi, M., Inzitari, R., Sbardell, D., Monaco, S., Pavoni, E., Gioia, M., Marini, S., Morlacchi, S., Sciandra, F., Castagnola, M. *et al.* (2009) Enzymatic processing of β-dystroglycan recombinant ectodomain by MMP-9: identification of the main cleavage site. *IUBMB Life*, **61**, 1143–1152.
32. Haas, T.L., Davis, J. and Madri, J.A. (1998) Three-dimensional type I collagen lattices induce coordinate expression of matrix metalloproteinases MT1-MMP and MMP-2 in microvascular endothelial cells. *J. Biol. Chem.*, **273**, 3604–3610.
33. Kuzuya, M., Kanda, S., Sasaki, T., Mori, N., Chen, X.W., Itoh, T., Itohara, S. and Iguchi, A. (2003) Deficiency of gelatinase A suppression smooth muscle cell invasion and development of experimental intimal hyperplasia. *Circulation*, **108**, 1375–1381.
34. Kinoh, H., Sato, H., Tsunezuka, Y., Takino, T., Kawashima, A., Okada, Y. and Seiki, M. (1996) MT-MMP, the cell surface activator of proMMP-2 (pro-gelatinase A), is expressed with its substrate in mouse tissue during embryogenesis. *J. Cell. Sci.*, **109**, 953–959.
35. Matsumoto, T. and Claesson-Welsh, L. (2001) VEGF receptor signal transduction. *Sci. STKE*, **112**, 1–17.
36. Germani, A., Carlo, A.D., Mangori, A., Straino, S., Giacinti, C., Turrini, P., Biglioli, P. and Capogrossi, C. (2003) Vascular endothelial growth factor modulates skeletal myoblast function. *Am. J. Pathol.*, **163**, 1417–1428.
37. Messina, S., Mazzeo, A., Bitto, A., Aguennouz, M., Migliorato, A., Pasquale, M.G., Minutoli, L., Altavilla, D., Zentilin, L., Giacca, M., Squandrito, F. and Vita, G. (2007) VEGF overexpression via adeno-associated virus gene transfer promotes skeletal muscle regeneration and enhances muscle function in *mdx* mice. *FASEB J.*, **21**, 3737–3746.
38. Arsic, N., Zacchigna, S., Zentilin, L., Ramirez-Correa, G., Pattarini, L., Salvi, A., Sinagra, G. and Giacca, M. (2004) Vascular endothelial growth factor stimulates skeletal muscle regeneration *in vivo*. *Mol. Ther.*, **10**, 844–854.
39. De Angelis, L., Berghella, L., Coletta, M., Lattanzi, L., Zanchi, M., Cusela-De Angelis, M.G., Ponzetto, C. and Cossu, G. (1999) Skeletal myogenic progenitors originating from embryonic dorsal aorta coexpress endothelial and myogenic markers and contribute to postnatal muscle growth and regeneration. *J. Cell Biol.*, **147**, 869–877.
40. Chetty, C., Lakka, S.S., Bhoopathi, P. and Rao, J. (2009) MMP-2 alters VEGF expression via αVβ3 integrin-mediated PI3K/AKT signaling in A549 lung cancer cells. *Int. J. Cancer*, **127**, 1081–1095.
41. Heizmann, C.W., Fritz, G. and Schafer, B.W. (2002) S100 proteins: structure, functions and pathology. *Front. Biosci.*, **7**, d1356–d1368.
42. Yong, H.Y. and Moon, A. (2007) Role of calcium-binding proteins, S100A8 and S100A9, in invasive phenotype of human gastric cancer cells. *Arch. Pharm. Res.*, **30**, 75–81.
43. van Lent, P.L., Grevers, L.C., Blom, A.B., Arntz, O.J., van de Loo, F.A., van der Kraan, P., Abdollahi-Roodsaz, S., Srikrishna, G., Freeze, H., Sloetjes, A. *et al.* (2008) Stimulation of chondrocyte-mediated cartilage destruction by S100A8 in experimental murine arthritis. *Arthritis Rheum.*, **58**, 3776–3787.
44. Lloyd, P.G., Yang, H.T. and Terjung, R.L. (2001) Arteriogenesis and angiogenesis in rat ischemic hindlimb: role of nitric oxide. *Am. J. Physiol. Heart Circ. Physiol.*, **281**, H2528–H2538.
45. Wehling, M., Spencer, M.J. and Tidball, J.G. (2001) A nitric oxide synthase transgene ameliorates muscular dystrophy in *mdx* mice. *J. Cell Biol.*, **155**, 123–131.
46. Ito, K., Kimura, S., Ozasa, S., Matsukura, M., Ikezawa, M., Yoshioka, K., Ueno, H., Suzuki, M., Araki, K., Yamamura, K. *et al.* (2006) Smooth muscle-specific dystrophin expression improves aberrant vasoregulation in *mdx* mice. *Hum. Mol. Genet.*, **15**, 2266–2275.

Downloaded from http://hmg.oxfordjournals.org/ at NCNP on May 16, 2012

47. Guggilam, A., Patel, K.P., Haque, M., Ebenezer, P.J., Kapusta, D.R. and Francis, J. (2008) Cytokine blockade attenuates sympathoexcitation in heart failure: cross-talk between nNOS, AT-1R and cytokines in the hypothalamic paraventricular nucleus. *Eur. J. Heart Fail.*, **10**, 625–634.
48. Ehlermann, P., Eggers, K., Bierhaus, A., Most, P., Weichenhan, D., Greten, J., Nawroth, P.P., Katus, H.A. and Remppis, A. (2006) Increased proinflammatory endothelial response to S100A8/A9 after preactivation through advanced glycation end products. *Cardiovasc. Diabetol.*, **5**, 6.
49. Lange, M., Nakano, Y., Traber, D.L., Hamahata, A., Esechie, A., Jonkam, C., Bansal, K., Traber, L.D. and Enkhbaatar, P. (2010) Role of different nitric oxide synthase isoforms in a murine model of acute lung injury and sepsis. *Biochem. Biophys. Res. Commun.*, **399**, 286–291.
50. Gebhardt, C., Nemeth, J., Angel, P. and Hess, J. (2006) S100A8 and S100A9 in inflammation and cancer. *Biochem. Pharmacol.*, **72**, 1622–1631.
51. Nauck, M., Karakiulakis, G., Perruchoud, A.P., Papakonstaninou, E. and Roth, M. (1998) Corticosteroid inhibit the expression of the vascular endothelial growth factor gene in human vascular smooth muscle cells. *Eur. J. Pharmacol.*, **341**, 309–315.
52. Pross, C., Farooq, M.M., Angle, N., Lane, J.S., Cerveira, J.J., Xavier, A.E., Freischlag, J.A., Law, R.E. and Gelabert, H.A. (2002) Dexamethasone inhibits vascular smooth muscle cell migration via modulation of matrix metalloproteinase activity. *J. Surg. Res.*, **102**, 57–62.
53. Menezes, L.G., Sobreira, C., Neder, L., Rodrigeus, A.L. Jr and Martinez, J.A.B. (2007) Creatine supplementation attenuates corticosteroid-induced muscle wasting and impairment of exercise performance in rats. *J. Appl. Physiol.*, **102**, 698–703.
54. Barel, M., Perez, O.A.B., Giozzet, V.A., Rafacho, A., Bosqueiro, J.R. and Amaral, S.L. (2010) Exercise training prevents hyperinsulinemia, muscular glycogen loss and muscle atrophy induced by dexamethasone treatment. *Eur. J. Appl. Physiol.*, **108**, 999–1007.
55. Amalfitano, A. and Chamberlain, J.S. (1996) The *mdx*-amplification-resistant mutation system assay, a simple and rapid polymerase chain reaction-based detection of the *mdx* allele. *Muscle Nerve*, **19**, 1549–1553.
56. Massa, R., Silvestri, G., Zeng, Y.C., Martorana, A., Sancesario, G. and Bernardi, G. (1997) Muscle regeneration in *mdx* mice: resistance to repeated necrosis is compatible with myofiber maturity. *Basic Appl. Myol.*, **7**, 387–394.
57. Gosselin, L.E., Williams, J.E., Personius, K. and Farkas, G.A. (2007) A comparison of factors associated with collagen metabolism in different skeletal muscles from dystrophic (*mdx*) mice: impact of pirfenidone. *Muscle Nerve*, **35**, 208–216.

Downloaded from http://hmg.oxfordjournals.org/ at NCNP on May 16, 2012

PEDIATRICS INTERNATIONAL Official Journal of the Japan Pediatric Society
Pediatrics International (2011) **53**, 524–529
doi: 10.1111/j.1442-200X.2011.03330.x

Original Article

Exon-skipping events in candidates for clinical trials of morpholino

Shiho Nakano,[1] Shiro Ozasa,[1] Kowashi Yoshioka,[1] Isao Fujii,[3] Kouichi Mitsui,[1] Keiko Nomura,[1] Hirofumi Kosuge,[1] Fumio Endo,[2] Makoto Matsukura[3] and Shigemi Kimura[1]

Departments of [1]Child Development and [2]Pediatrics, Kumamoto University Graduate School, and [3]Laboratory of Clinical Pharmacology and Therapeutics, Faculty of Pharmaceutical Sciences, Sojo University, Kumamoto, Japan

Abstract ***Background***: Duchenne muscular dystrophy (DMD) and Becker muscular dystrophy (BMD) are caused by abnormalities in the *DMD* gene. The majority of DMD patients have out-of-frame deletion(s), which disrupt the reading frame; while some cases of DMD are caused by duplication or nonsense mutation(s). Most patients with BMD have in-frame deletion(s), which preserve the reading frame. The phenotype of BMD is generally milder than that of DMD. Antisense morpholino-mediated exon skipping, which changes out-of-frame deletions to in-frame deletions, is a promising therapeutic approach for DMD. It is necessary, however, to confirm the exon-skipping event in cells of DMD patients before the clinical trial.

Methods: Fibroblasts isolated from four DMD patients were induced to differentiate into the myogenic lineage by infection with Ad.CAGMyoD. The cells were then transfected with two types of morpholino. The exon-skipping event was analyzed on reverse transcription–polymerase chain reaction.

Results: Morpholino B30, which is located at the splicing enhancer of exon 51 of the *DMD* gene, yielded the desired exon 51-skipping event in all deletion patterns of cells tested. Morpholino I25, which is located at the exon donor, induced two different exon-skipping patterns, which are total or partial exon 51-skipping events. According to the sequence analysis, the unexpected unskipped regions were the 95 bp section and the 188 bp section of exon 51, showing that the cryptic splicing donor was newly produced with I25. Unfortunately, these cryptic splicing donors gave rise to out-of-frame patterns. Based on these *in vitro* results, B30 would presumably be an effective therapy. Interestingly, the cocktail of B30 and I25 appeared to yield a more efficient exon 51-skipping event.

Conclusion: An *in vitro* system was developed that could easily screen the effectiveness of antisense sequences and identify good candidates for therapy with morpholino.

Key words Duchenne muscular dystrophy, dystrophin, exon skipping, fibroblast, morpholino.

Duchenne muscular dystrophy (DMD) is caused by defective expression of the *DMD* gene, resulting in the absence of the dystrophin protein in muscle fibers.[1] Approximately 60% of DMD/Becker muscular dystrophy (BMD) patients have deletions in the *DMD* gene itself, while the remaining 40% of patients have duplication, small deletions or point mutations in the region that encodes the gene.[2–7] DMD, which manifests as a severe muscle weakness phenotype, results from an out-of-frame deletion(s) in the *DMD* gene, leading to prematurely truncated, dysfunctional dystrophin.[8] In contrast, BMD, which results from an in-frame deletion(s) in the *DMD* gene, leads to the synthesis of internally defective but largely functional dystrophin. Thus, the muscle weakness seen in BMD is generally milder than that of DMD. Ninety percent of DMD and BMD patients seem to fit this rule.[2] Van Deutekom *et al.*, Wilton *et al.*, Dunckley *et al.* and Takeshima *et al.* reported promising results for a genetic therapy aimed at restoring the reading frame of the dystrophin pre-mRNA in cells from the mdx mouse model and from DMD patients.[9–12] The strategy corrects the reading frame by inducing the skipping of specific exons during pre-mRNA splicing by using antisense oligonucleotides (AON) that interfere with the splicing of the targeted exons. This restoration may convert a Duchenne phenotype into a Becker phenotype.[13]

Phosphorodiamidate morpholino oligonucleotides (PMO) are a type of AON in which the phosphodiester bond is replaced by a phosphorodiamidate linkage and the ribose is replaced by a morpholino moiety. PMO seem most promising because they have higher affinity to their target nucleic acid sequences and greater resistance to degradation than conventional nucleic acids.[14] It is hard, however, to transfect PMO into cells *in vitro*, because they are non-ionic.[15] Therefore, there are major limitations in evaluating PMO in cultured cells.[16]

Alter *et al.* showed that weekly i.v. injections of PMO induce the expression of functional levels of dystrophin in skeletal muscles of the dystrophic mdx mouse, resulting in improved

Correspondence: Shigemi Kimura, MD, PhD, Department of Child Development, Kumamoto University Graduate School, 1-1-1 Honjo, Kumamoto 860-0811, Japan. Email: kimusige@kumamoto-u.ac.jp

Received 9 April 2010; revised 5 November 2010; accepted 30 November 2010.

© 2011 The Authors
Pediatrics International © 2011 Japan Pediatric Society

muscle function.[17] Yokota *et al.* reported that i.v. injections of a three-morpholino cocktail into DMD dogs induced therapeutic levels of dystrophin expression throughout the body (the average level was approx. 26% of the normal level), and the phenotype was improved.[18] Intramuscular injection of antisense oligonucleotide PRO051 (2-*O*-methyl oligonucleotides) and AVI-4658 (morpholino oligomer) induced dystrophin synthesis in DMD patients with suitable mutations, suggesting that further studies might be feasible.[19,20]

The exclusion of target exon 51 is predictive of the restoration of the DMD open reading frame (ORF) in 17% of DMD patients with a deletion mutation.[21] Exon 51 is the target for intervention in the present experimental design.[22] Fortunately, the BMD patients with in-frame deletions (exons 45–51 and 50–51) that encompass exon 51 are reported to have a mild phenotype.[23] Although this method is promising, 10% of the mutations recorded in the Leiden DMD mutation databases do not follow the reading-frame rule.[2] Prior to the initiation of clinical treatment, the correct exon-skipping events with the antisense sequence must be confirmed, because the sequences are different between human patients and animal models, and a small percentage of patients with the Duchenne type actually have an in-frame deletion in the *DMD* gene.[2] Therefore, we developed a system that can easily screen antisense sequences and identify patients who are eligible for the therapy.

Methods

Strategy

Fibroblasts isolated from DMD patients were induced to differentiate into the myogenic lineage by infection with Ad.CAG-MyoD, an adenoviral vector encoding MyoD regulated by the CAG promoter.[24,25] The cells were then transfected with two PMO, termed B30 and I25 by Arechavala-Gomeza *et al.*,[22] which were designed to induce exon 51 skipping. B30 is located at the splicing enhancer of exon 51 of the *DMD* gene, and I25 is located at the exon donor. B30 was reported to be the most efficient inducer of exon 51 skipping, while I25 was a poor inducer that yielded a faint exon 51-skipping event. We analyzed the exon-skipping event on reverse transcription–polymerase chain reaction (RT-PCR) after transfection.

Cell culture and AON transfection

The study protocol was approved by the institutional ethics committee of Kumamoto University. Human primary fibroblasts were isolated from the buttocks or upper arms of four DMD patients (ages 10, 18, 8, and 12 years) who had deletions of exons 45–50, 48–50, 49–50, and 50, respectively, in the *DMD* gene. Patients with deletions of exons 45–50 and 49–50 can walk by themselves, while patients with deletions of 48–50 and 50 require the use of a wheelchair. The range of deletions was determined on multiplex ligation-dependent probe amplification of the *DMD* gene (Mitsubishi Kagaku Bio-clinical Lab., Tokyo, Japan). A total of 4×10^5 cells were seeded onto a 6 cm dish 1 day before infection. Cells were cultured in growth medium (Dulbecco's modified Eagle's medium [DMEM]; Invitrogen, Carlsbad, CA, USA) with 10% fetal bovine serum (FBS; Moregate Biotech, Bulimba, Qld, Australia) and were infected with Ad.CAGMyoD at a multiplicity of infection of 20 (total amount, 1.33 μL of 6×10^9 PFU/mL) in 1 mL of FCS-free Hanks' Balanced Salt solution (HBSS; Invitrogen) for 2 h. During the infection, the HBSS was occasionally stirred. Sequentially, 3 mL of growth medium was added onto the dish. On the following day, the culture medium was replaced with differentiation medium (DMEM plus 2% FBS). When myoblasts fused to form myotubes, usually after 4 days,[24,25] the differentiated cells were transfected with 10 μmol/L PMO (10 μmol/L B30, 10 μmol/L I25, or 5 μmol/L of each) using Endo-Porter according to the manufacturer's instructions (Gene Tools, Philomath, OR, USA). The standard control (Gene Tools) was used for the negative control under each condition. At 7–8 days after infection, RNA was isolated from the cells for RT-PCR.

Nested RT-PCR

Primary PCR consisted of 38 cycles of 94°C (1 min), 55°C (1 min) and 72°C (3 min) with the pairs of primers described here (Figs 1,2). Ten 1 μL aliquots of the primary reaction products were then re-amplified in nested PCR consisting of 20 cycles of 94°C (1 min), 55°C (1 min) and 72°C (3 min) with the following primers (Figs 1,2): for the patient with the exon 45–50 deletion, exon 44-f1 (5′-gcgatttgacagatctgttg-3′) and exon 53-r (5′-aact gttgcctccggttctg-3′) for the first PCR and exon 44-f2 (5′-ggc ggcgttttcattatgatat-3′) and exon 52-r(5′-ttccaactggggacgcctctgttc-3′) for the second PCR; for the patient with a deletion of exon 48–50, exon 46-f (5′-gctagtatcccacttgaacctg-3′) and exon 53-r for the first PCR, and exon 47-f (5′-tgcgccagggaattctcaaa-3′) and exon 52-r for the second PCR; and for the patients with the exon 49–50 deletion and the exon 50 deletion, exon 47-f and exon 53-r for the first PCR and exon 48-f (5′-gcttgaagaccttgaagagc-3′) and exon 52-r for the second PCR. PCR products were analyzed on 3% agarose gels.

Sequence analysis

DNA fragments amplified on PCR were sequenced with the dideoxy chain termination method using an automated sequencer (ABI Prism 310; Applied Biosystems, Tokyo, Japan) following the standard protocol.

Results

Differentiation of fibroblasts into myotubes with Ad.CAGMyoD

Fibroblasts (Fig. 1a,b) began to fuse together at 4 days after infection and differentiate into myotubes at 6 days after infection. On RT-PCR dystrophin expression was detected from at least 7–8 days after infection (Fig. 1c).

Exon 51 skipping after Endo-Porter–mediated transfection of 10 μmol/L PMO

Fibroblasts with deletions of exon 45–50, 48–50, 49–50 and 50 of the DMD gene were used to check the exon 51-skipping event after being stably transfected with 10 μmol/L B30 or I25, or 5 μmol/L of each, with Endo-Porter. RT-PCR showed that the

© 2011 The Authors
Pediatrics International © 2011 Japan Pediatric Society

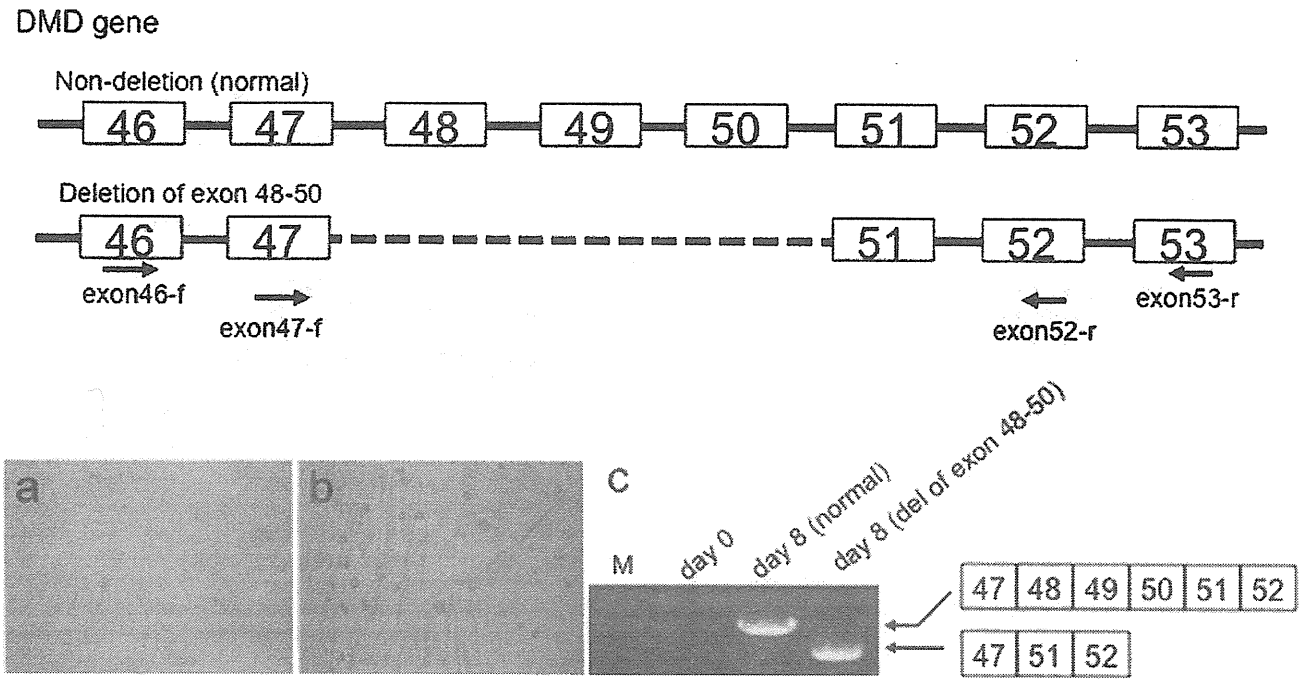

Fig. 1 Dystrophin expression from fibroblast into muscle lineage after infection of Ad.CAGMyoD. Upper panels, normal gene without deletions and the locations of the deletions of exon 48–50 in the Duchenne muscular dystrophy (DMD) gene. Arrows, locations of reverse transcription–polymerase chain reaction (RT-PCR) primers. (a) Non-Ad.CAGMyoD-infected non-deleted fibroblasts. (b) Fibroblasts at 8 days after infection of Ad.CAGMyoD. The fibroblasts were fused together. (c) Dystrophin expression was not detected in non-infected fibroblasts (day 0) but was detected in fibroblasts with non-deletion (normal) and deletion of exon 48–50 at 8 days after infection. M, DNA Molecular Weight Marker X (Roche, Penzberg, Germany).

transfection of B30 always yielded the exon 51-skipping event (Fig. 2). The size of the RT-PCR bands from cells with the exon 45–50 deletion, the exon 48–50 deletion, the exon 49–50 deletion and the exon 50 deletion was 164, 170, 154 and 256 bp, respectively. In the case of I25 transfection, cells with the exon 45–50 deletion yielded the long partial exon 51-skipped transcript (352 bp) and the exon 51-skipped transcript (164 bp; Fig. 2a); cells with the exon 48–50 deletion yielded the long partial exon 51-skipped transcript (358 bp) and the short partial exon 51-skipped transcript (265 bp; Fig. 2b); cells with the exon 49–50 deletion yielded the long partial exon 51-skipped transcript (342 bp) and the exon 51-skipped transcript (154 bp; Fig. 2c); and cells with the exon 50 deletion yielded all sizes of transcripts (the 444 bp long partial exon 51-skipped transcript; the 351 bp short partial exon 51-skipped transcript; and the 256 bp exon 51-skipped transcript; Fig. 2d). Interestingly, in the case of cells with the exon 48–50 deletion, the non-exon 51-skipped band was absent; only the long and short partial exon 51-skipped transcripts were observed (Fig. 2b).

When a cocktail of B30 and I25 was transfected, cells with the exon 49–50 deletion yielded the long partial exon 51-skipped transcript and the exon 51-skipped transcript, and cells with the exon 50 deletion yielded all types of transcripts (Fig. 2c,d). The density of the exon 51-skipped band after transfection with the cocktail of B30 and I25 was greater than the density of the non-exon 51-skipped band. Interestingly, when I25 was used, the long partial exon 51-skipped transcripts were always observed (Fig. 2).

Sequence analysis of short and long fragments

Reverse transcription–polymerase chain reaction of cells transfected with I25 showed two kinds of bands different to the non-exon 51-skipped transcript and the exon 51-skipped transcript. According to the sequence analysis, the short fragment contained a 95 bp section of exon 51 (Fig. 3a), and the long fragment contained a 188 bp section of exon 51 (Fig. 3b). The 3′ end of the 95 bp section is GAG|GTA (exon| intron), which partially coincides with the consensus sequence of the splicing donor, C/AAG|GTA/G (exon| intron), without the first G of GAG in the 3′ end of the exon (Fig. 3a).[26,27] The 3′ end of the 188 bp section is ATG|GTG (exon| intron), which also partially coincides with the consensus sequence of the splicing donor, C/AAG|GTA/G (exon| intron), without the second T in ATG of the 3′ end of the exon (Fig. 3b). Thus, both segments appear to be cryptic splicing donors.

Discussion

In the present study we show that it is important to check the exon-skipping event *in vitro* by using patient fibroblasts before the initiation of therapy. Generally, PMO are not suitable for *in vitro* experiments,[15,16] but they are powerful tools for exon-skipping therapy.

© 2011 The Authors
Pediatrics International © 2011 Japan Pediatric Society

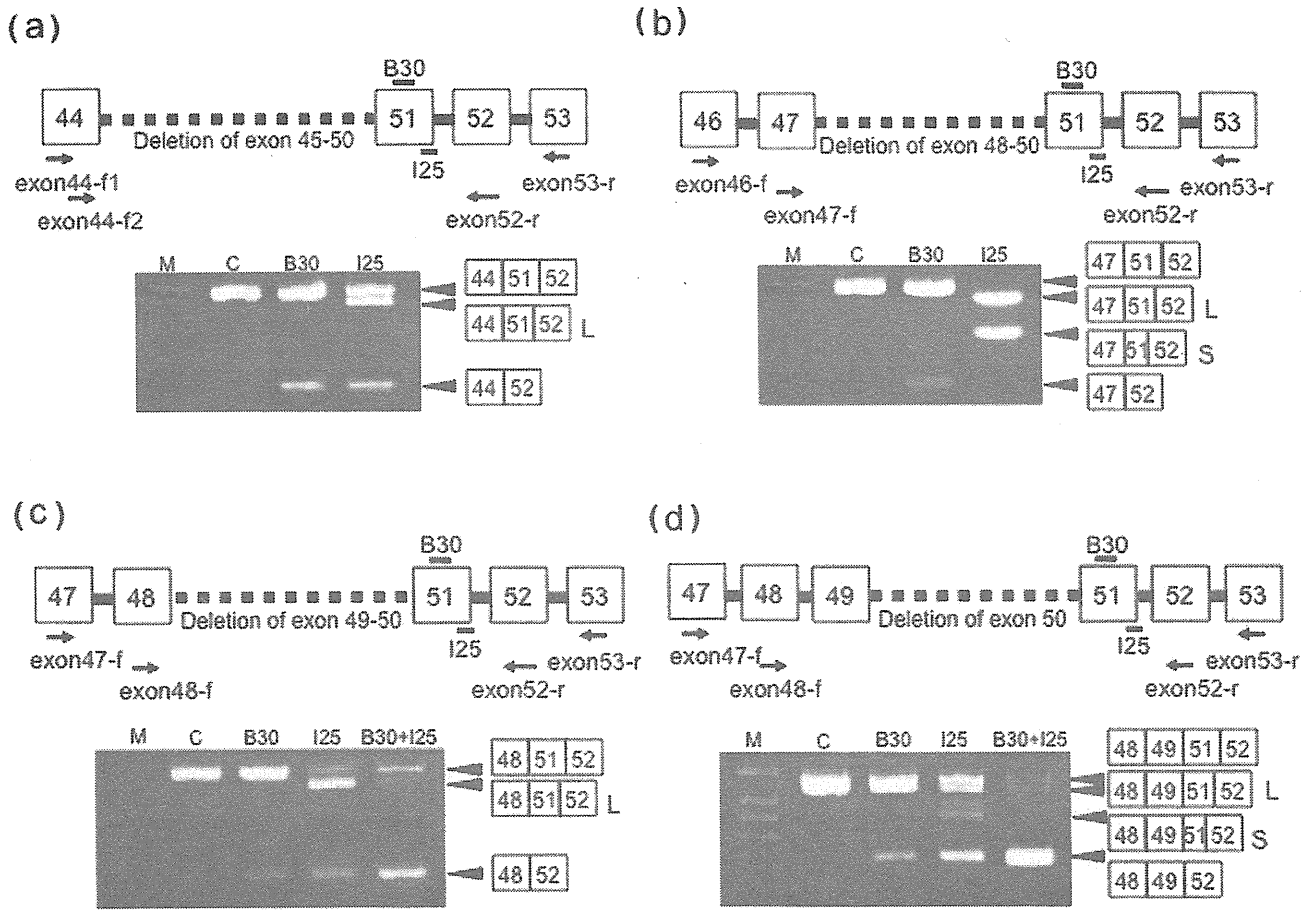

Fig. 2 Endo-Porter transfection with 10 μmol/L of antisense morpholino. The Endo-Porter-mediated transfection of 10 μmol/L of phosphorodiamidate morpholino oligonucleotide (PMO) was stable. Upper panels, locations of the deletions in the Duchenne muscular dystrophy (DMD) gene. The deletions were (a) exons 45–50, (b) 48–50, (c) 49–50 and (d) 50. Arrows, locations of the reverse transcription–polymerase chain reaction (RT-PCR) primers. The positions of B30 and I25, the two PMO, are indicated. (a–d) RT-PCR of RNA isolated from fibroblasts that differentiated into muscle lineage and were subjected to Endo-Porter-mediated transfection of morpholino. The illustrations to the right of the gel show the pattern of exon-skipping. (a–d) The exon 51-skipping event was also correctly detected in cells transfected with B30. In contrast, RT-PCR of I25-transfected cells produced two kinds of bands, a long and a short partial exon 51-skipped transcript. (c,d) The transfection of a cocktail of B30 and I25 yielded the skipping patterns of B30 plus I25. Interestingly, the cocktail appeared to mediate a more efficient exon 51-skipping event. C, transfection of standard for a negative control; L, long partial exon 51-skipped transcript; M, DNA Molecular Weight Marker X (Roche, Penzberg, Germany); S, short partial exon 51-skipped transcript.

We initially performed single RT-PCR to detect exon skipping, but the results showed many extra bands. These extra bands might be caused by repeated sequences of the rod domain of the *DMD* gene. Therefore, we performed nested RT-PCR. After transfection of B30, only the exon 51-skipping event was observed. In contrast, after transfection of I25, we detected two kinds of longer partial exon 51-skipped transcripts that were different from the non-exon 51 and exon 51-skipped transcripts. These two types of partial exon 51-skipped transcripts were also observed in the Aartsma-Rus *et al.* study after I25 was injected i.m. into a transgenic mouse expressing a complete copy of the human *DMD* gene.[2] The authors, however, did not provide a clear description of these skipped transcripts. Sequence analysis in the present study produced two bands, a 95 bp band and a 188 bp band, which each included part of exon 51, because I25 produced two cryptic splicing donors on exon 51. Unfortunately, these cryptic splicing donors resulted in an out-of-frame deletion. Therefore, we should check the consensus sequence of a splicing donor when we design sequences for antisense therapy. Such various exon-skipping patterns might be explained by differences in differentiation, because the PMO were transfected into cells in the differential stage from fibroblast to myotube. In addition, the different exon-skipping patterns were also caused by differences in the deletion patterns of the *DMD* gene, which is difficult to explain and suggests a difference in the exon-skipping pattern between wild type and the DMD dog.[18]

The transfection of a cocktail of B30 and I25 yielded the skipping pattern of B30 plus the pattern of I25. Interestingly, the cocktail appeared to yield a more efficient exon 51-skipping event than an equivalent total amount of one PMO. Thus, it seems

© 2011 The Authors
Pediatrics International © 2011 Japan Pediatric Society

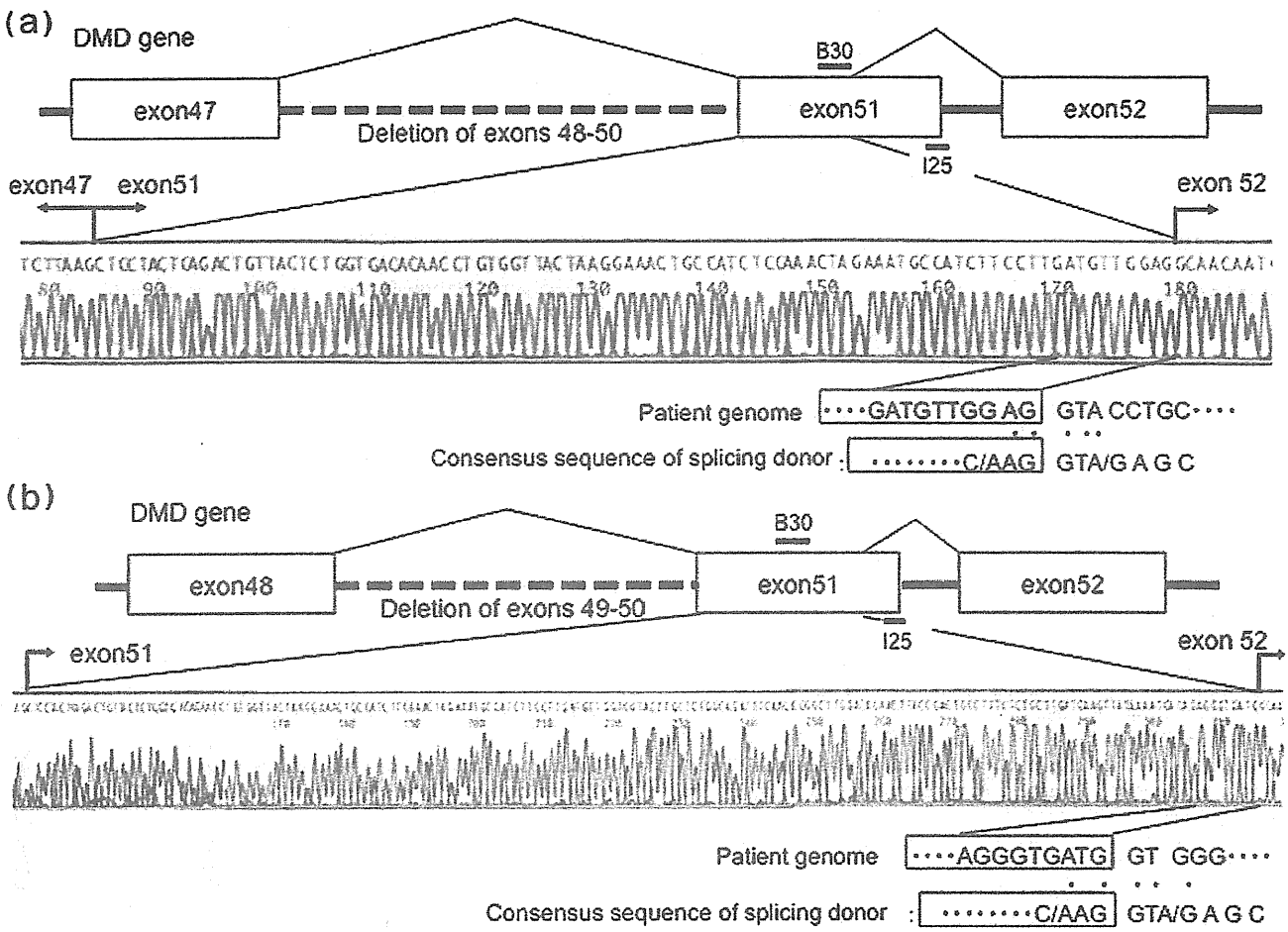

Fig. 3 Sequence analysis of short and long fragments after transfection with I25. (a,b) Upper panels, locations of deletions in the Duchenne muscular dystrophy (DMD) gene and the splicing pattern. The bottom schema shows the border of cryptic donor. Dots, nucleotides that are identical to the consensus sequence of the splicing donor. Boxes, exons. (a,b) The short fragment (short partial exon 51-skipped transcript) and the long fragment (long partial exon 51-skipped transcript) included 95 and 188 bp of exon 51, respectively, because the cryptic splicing donor was produced.

that B30 and I25 together inhibited the splicing of exon 51 more than either B30 or I25 alone.

We checked the exonic splicing enhancer (ESE) scores of the sequences of B30 and I25. The sequence motives recognized by the four most abundant SR proteins (SF2/ASF, SC35, SRp40 and SRp55) are implemented in the ESEfinder software. The scores/threshold of the SF2/ASF, SC35, SRp40, and SRp55 motif of B30 were 0.31027/1.956, 1.47752/ 2.383, .34852/2.67 and 0.41398/2.676, respectively. For I25, the scores were 3.09235/1.956, 0.48692/ 2.383, 1.52791/2.67, and 1.02577/2.676, respectively. The I25 ESE score is higher than that of B30. The score sometimes did not represent the true ESE.[28]

Aartsma-Rus *et al.* noted that not every effective PMO has high values of ESE score for SR protein binding sites and some ineffective PMO do have high values. Furthermore, ESEfinder predicts putative ESE sites for the most abundant SR proteins only.[29] So several important variables, such as the local sequence context, the splice-site strengths, the position of the ESE along the exon and the presence of silencer elements, are likely to play a significant role in ESE activity.[28] We calculated ESE score, but the skipping efficiency does not accord with score like in other articles.

In conclusion, B30 is suitable for clinical therapy, because transfection with B30 consistently yielded only the exon 51-skipped band. I25 is not suitable, because various undesired transcripts were detected after its transfection. Chaouch *et al.* also analyzed the dystrophin expression in immortalized fibroblasts of a DMD patient by using engineered U7 small nuclear RNAs harboring the antisense sequence required to restore an in-frame dystrophin mRNA by skipping exon 51.[30]

Our strategy is a faster and easier method for the screening of exon skipping in each patient, and it allows for many kinds of PMO to be checked prior to the initiation of therapy.

We conclude that clinical trials of PMO should be performed with prior *in vitro* experiments using cellular systems to check the possible effectiveness in patients.

© 2011 The Authors
Pediatrics International © 2011 Japan Pediatric Society

Acknowledgments

The authors thank Ryan Pruchnic (Cook MyoSite, Pittsburgh, PA, USA) for his assistance. This study was supported by a research grant (19-7) for nervous and mental disorders from the Ministry of Health, Labour, and Welfare, a grant for research in brain science from the Ministry of Health, Labour and Welfare, and a grant from the Ministry of Education, Science, Culture and Sports of Japan.

References

1 Hoffman EP, Brown RH Jr, Kunkel LM. Dystrophin: The protein product of the Duchenne muscular dystrophy locus. *Cell* 1987; **51**: 919–28.
2 Aartsma-Rus A, Van Deutekom JC, Fokkema IF, Van Ommen GJ, Den Dunnen JT. Entries in the Leiden Duchenne muscular dystrophy mutation database: An overview of mutation types and paradoxical cases that confirm the reading-frame rule. *Muscle Nerve* 2006; **34**: 135–44.
3 De Angelis FG, Sthandier O, Berarducci B *et al.* Chimeric snRNA molecules carrying antisense sequences against the splice junctions of exon 51 of the dystrophin pre-mRNA induce exon skipping and restoration of a dystrophin synthesis in Delta 48–50 DMD cells. *Proc. Natl Acad. Sci. USA* 2002; **99**: 9456–61.
4 Mann CJ, Honeyman K, Cheng AJ *et al.* Antisense-induced exon skipping and synthesis of dystrophin in the mdx mouse. *Proc. Natl Acad. Sci. USA* 2001; **98**: 42–7.
5 Gillard EF, Chamberlain JS, Murphy EG *et al.* Molecular and phenotypic analysis of patients with deletions within the deletion-rich region of the Duchenne muscular dystrophy (DMD) gene. *Am. J. Hum. Genet.* 1989; **45**: 507–20.
6 Forrest SM, Cross GS, Flint T, Speer A, Robson KJ, Davies KE. Further studies of gene deletions that cause Duchenne and Becker muscular dystrophies. *Genomics* 1988; **2**: 109–14.
7 Lindlof M, Kiuru A, Kaariainen H *et al.* Gene deletions in X-linked muscular dystrophy. *Am. J. Hum. Genet.* 1989; **44**: 496–503.
8 Koenig M, Beggs AH, Moyer M *et al.* The molecular basis for Duchenne versus Becker muscular dystrophy: Correlation of severity with type of deletion. *Am. J. Hum. Genet.* 1989; **45**: 498–506.
9 van Deutekom JC, Bremmer-Bout M, Janson AA *et al.* Antisense-induced exon skipping restores dystrophin expression in DMD patient derived muscle cells. *Hum. Mol. Genet.* 2001; **10**: 1547–54.
10 Wilton SD, Lloyd F, Carville K *et al.* Specific removal of the nonsense mutation from the mdx dystrophin mRNA using antisense oligonucleotides. *Neuromuscul. Disord.* 1999; **9**: 330–38.
11 Dunckley MG, Manoharan M, Villiet P, Eperon IC, Dickson G. Modification of splicing in the dystrophin gene in cultured Mdx muscle cells by antisense oligoribonucleotides. *Hum. Mol. Genet.* 1998; **7**: 1083–90.
12 Takeshima Y, Wada H, Yagi M *et al.* Oligonucleotides against a splicing enhancer sequence led to dystrophin production in muscle cells from a Duchenne muscular dystrophy patient. *Brain Dev.* 2001; **23**: 788–90.
13 Aartsma-Rus A, Bremmer-Bout M, Janson AA, den Dunnen JT, van Ommen GJ, van Deutekom JC. Targeted exon skipping as a potential gene correction therapy for Duchenne muscular dystrophy. *Neuromuscul. Disord.* 2002; **12** (Suppl. 1): S71–7.
14 Sazani P, Gemignani F, Kang SH *et al.* Systemically delivered antisense oligomers upregulate gene expression in mouse tissues. *Nat. Biotechnol.* 2002; **20**: 1228–33.
15 Summerton J, Weller D. Morpholino antisense oligomers: Design, preparation, and properties. *Antisense Nucleic Acid Drug Dev.* 1997; **7**: 187–95.
16 Aartsma-Rus A, Kaman WE, Bremmer-Bout M *et al.* Comparative analysis of antisense oligonucleotide analogs for targeted DMD exon 46 skipping in muscle cells. *Gene Ther.* 2004; **11**: 1391–8.
17 Alter J, Lou F, Rabinowitz A *et al.* Systemic delivery of morpholino oligonucleotide restores dystrophin expression bodywide and improves dystrophic pathology. *Nat. Med.* 2006; **12**: 175–7.
18 Yokota T, Lu QL, Partridge T *et al.* Efficacy of systemic morpholino exon-skipping in Duchenne dystrophy dogs. *Ann. Neurol.* 2009; **65**: 667–76.
19 Kinali M, Arechavala-Gomeza V, Feng L *et al.* Local restoration of dystrophin expression with the morpholino oligomer AVI-4658 in Duchenne muscular dystrophy: A single-blind, placebo-controlled, dose-escalation, proof-of-concept study. *Lancet Neurol.* 2009; **8**: 918–28.
20 van Deutekom JC, Janson AA, Ginjaar IB *et al.* Local dystrophin restoration with antisense oligonucleotide PRO051. *N. Engl. J. Med.* 2007; **357**: 2677–86.
21 van Deutekom JC, van Ommen GJ. Advances in Duchenne muscular dystrophy gene therapy. *Nat. Rev. Genet.* 2003; **4**: 774–83.
22 Arechavala-Gomeza V, Graham IR, Popplewell LJ *et al.* Comparative analysis of antisense oligonucleotide sequences for targeted skipping of exon 51 during dystrophin pre-mRNA splicing in human muscle. *Hum. Gene. Ther.* 2007; **18**: 798–810.
23 Helderman-van den Enden AT, Straathof CS, Aartsma-Rus A *et al.* Becker muscular dystrophy patients with deletions around exon 51; a promising outlook for exon skipping therapy in Duchenne patients. *Neuromuscul. Disord.* 2010; **20**: 251–4.
24 Fujii I, Matsukura M, Ikezawa M, Suzuki S, Shimada T, Miike T. Adenoviral mediated MyoD gene transfer into fibroblasts: Myogenic disease diagnosis. *Brain Dev.* 2006; **28**: 420–25.
25 Kimura S, Ito K, Miyagi T *et al.* A novel approach to identify Duchenne muscular dystrophy patients for aminoglycoside antibiotics therapy. *Brain Dev.* 2005; **27**: 400–5.
26 Horowitz DS, Krainer AR. Mechanisms for selecting 5′ splice sites in mammalian pre-mRNA splicing. *Trends Genet.* 1994; **10**: 100–6.
27 Milasin J, Muntoni F, Severini GM *et al.* A point mutation in the 5′ splice site of the dystrophin gene first intron responsible for X-linked dilated cardiomyopathy. *Hum. Mol. Genet.* 1996; **5**: 73–9.
28 Cartegni L, Wang J, Zhu Z, Zhang MQ, Krainer AR. ESEfinder: A web resource to identify exonic splicing enhancers. *Nucleic Acids Res.* 2003; **31**: 3568–71.
29 Aartsma-Rus A, De Winter CL, Janson AA *et al.* Functional analysis of 114 exon-internal AONs for targeted DMD exon skipping: Indication for steric hindrance of SR protein binding sites. *Oligonucleotides* 2005; **15**: 284–97.
30 Chaouch S, Mouly V, Goyenvalle A *et al.* Immortalized skin fibroblasts expressing conditional MyoD as a renewable and reliable source of converted human muscle cells to assess therapeutic strategies for muscular dystrophies: Validation of an exon-skipping approach to restore dystrophin in Duchenne muscular dystrophy cells. *Hum. Gene. Ther.* 2009; **20**: 784–90.

© 2011 The Authors
Pediatrics International © 2011 Japan Pediatric Society

Effective Drug Delivery System for Duchenne Muscular Dystrophy Using Hybrid Liposomes Including Gentamicin along with Reduced Toxicity

Mamiko YUKIHARA,[a] Kaori ITO,[b] Osamu TANOUE,[a] Koichi GOTO,[a] Taku MATSUSHITA,[a] Yoko MATSUMOTO,[a] Masako MASUDA,[c] Shigemi KIMURA,*[,b] and Ryuichi UEOKA*[,a]

[a] *Division of Applied Life Science, Graduate School of Engineering, Sojo University; 4–22–1 Ikeda, Kumamoto 860–0082, Japan:* [b] *Department of Child Development, Kumamoto University Graduate School; and* [c] *Department of Otolaryngology, Kumamoto University Graduate School; 1–1–1 Honjo, Kumamoto 860–0811, Japan.*

Received December 14, 2010; accepted January 28, 2011; published online February 7, 2011

It is known that gentamicin (GM) could be a possible treatment for Duchenne Muscular Dystrophy (DMD). However, GM therapy has been hindered by several problems such as severe side effects of GM. In order to resolve these problems, we developed the drug delivery system (DDS) of GM using hybrid liposomes (HL) composed of L-α-dimyristoylphosphatidylcholine (DMPC) and polyoxyethylene(23) lauryl ether ($C_{12}(EO)_{23}$). The hydrodynamic diameters of HL including GM (GM-HL) were 60—90 nm with a narrow range of the size distribution and the sizes were kept almost constant for over 4 weeks, suggesting that GM-HL could avoid the reticuloendothelial system *in vivo*. Furthermore, GM-HL accumulated more to the skeletal muscle cells of X chromosome-linked muscular distrophy (mdx) mice as compared to those of normal mice. Significantly, we succeeded in increasing dystrophin positive fibers in skeletal muscle cells of mdx mice using GM-HL along with the reduction of ototoxicity. It is suggested that GM should be carried more efficiently into the muscular cells of mdx mice by HL. These results indicate that HL could be an effective carrier in the DDS of GM therapy for DMD.

Key words Duchenne muscular dystrophy; hybrid liposome; gentamicin; drug delivery system; X chromosome-linked muscular distrophy mouse

Duchenne/Becker muscular dystrophy (DMD/BMD) is caused by a defective expression of the dystrophin gene resulting in the absence of the dystrophin protein in muscle fibers.[1,2] Approximately 60% of DMD/BMD patients have deletions in the dystrophin gene itself,[3—5] while the remaining 40% have small deletions or point mutations in the region that encodes the gene. Furthermore, nonsense mutations located within the gene account for approximately 5—13% of the muscular dystrophies.[6,7]

Aminoglycoside antibiotics such as gentamicin (GM) had the ability to allow the ribosome to read through a premature-termination codon of the dystrophin gene, which prevented normal translation of dystrophin protein.[8,9] Barton-Davis *et al.* demonstrated the possibility of treating X chromosome-linked muscular distrophy (mdx) mouse, which was an animal model for DMD that possessed a nonsense mutation in the dystrophin gene, with GM *in vivo*.[10] They used GM to suppress the nonsense mutations and could restore dystrophin expression successfully in mdx mouse. However, the GM therapy has been hindered by several problems such as severe side effects of GM, especially nephrotoxicity and ototoxicity, the poor delivery profile to muscle tissue, and short half-life in blood. Recently, the phase 2b clinical trial of PTC 124 (3-[5-(2-fluorophenyl)-[1,2,4]oxadiazol-3-yl]-benzoic acid),[11] which is a new drug to induce reading through a premature-termination codon without clear side-effects, showed that the primary endpoint of the change in 6 min walk distance tests did not reach any statistical significance within the 48 weeks duration of the study according to Genzyme corporation announcement.[12]

Therefore, to overcome these inadequacies of GM therapy for DMD, we encapsulated GM in hybrid liposomes (HL) for the delivery system. HL can be prepared by just the sonication of vesicular and micellar molecules in a buffer solution.[13,14] HL are free from any contamination with organic solvents and remain stable for longer periods. The physical properties of these liposomes such as size, membrane fluidity, phase transition temperature, and hydrophobicity can be controlled by changing the constituents and compositional ratios. In the course of our study for HL, the following interesting results have been obtained. (a) Stereochemical control of the enantioselective hydrolysis of amino acid esters could be established by temperature regulation and changing the composition of the HL.[12,13] (b) Inhibitory effects of HL including antitumor drugs,[15] sugar surfactants,[16] or polyunsaturated fatty acids[17] have been observed on the growth of tumor cells *in vitro* and *in vivo*. (c) High inhibitory effects of HL on the growth of tumor cells along with the induction of apoptosis *in vitro*[18] and *in vivo*[19] have been obtained without using drugs.[20] Successful clinical chemotherapy with drug-free HL to patients with lymphoma has been reported after passing the committee of bioethics.[21] (d) A good correlation between membrane fluidity of HL and antitumor effects on the growth of tumor cells has been observed.[22] These studies indicate that HL had no cytotoxicity and could be effective carriers for improving solubilization and stabilization of hydrophilic[23] and hydrophobic agents in the drug delivery system (DDS).

In this study, we reported the therapeutic effects of HL including GM (GM-HL) on the mdx mice *in vivo*. The reduction of side effects of GM-HL is also discussed on the basis of the results from auditory brainstem response (ABR) tests and biodistribution analysis of HL.

MATERIALS AND METHODS

Preparation of HL, GM-HL and NBD-HL HL were prepared by sonication of a mixture containing 95 mol% L-α-dimyristoylphosphatidylcholine (DMPC) (NOF, Tokyo, Japan) and 5 mol% polyoxyethylene(23) lauryl ether ($C_{12}(EO)_{23}$) (Sigma-Aldrich, St. Louis, MO, U.S.A.) using a bath type soni-

* To whom correspondence should be addressed. e-mail: ueoka@life.sojo-u.ac.jp; kimusige@kumamoto-u.ac.jp © 2011 Pharmaceutical Society of Japan

cator (VS-N300, VELVO-CLEAR, Tokyo, Japan) in phosphate buffered saline (PBS(−)) at 45 °C with 300 W, and filtered with a 0.20 μm cellulose acetate filter (ADVANTEC, Tokyo, Japan). HL including GM (GM-HL) or 1-palmitoyl-2-[12-[(7-nitro-2-1,3-benzoxadiazol-4-yl)amino]dodecanoyl]-*sn*-glycero-3-phosphocholine (NBDPC) (NBD-HL) were prepared with GM (Schering-Plough, Kenilworth, NJ, U.S.A.) or NBDPC (Avanti Polar Lipids, Alabaster, AL, U.S.A.) by the same method of HL, respectively.

Dynamic Light Scattering Measurement Apparent mean hydrodynamic diameters (d_{hy}) of HL, GM-HL and NBD-HL were measured using a light scattering spectrometer (ELS-8000, Otsuka Electronics, Osaka, Japan) with a He–Ne laser light source (633 nm). The diameter was calculated by Stokes–Einstein equation (Eq. (1)),

$$d_{hy} = (\kappa T)/(3\pi\eta D) \quad (1)$$

where κ is Boltzmann constant, T is the absolute temperature, η is the viscosity of the solvent and D is the diffusion coefficient.

Electron Microscopy Electron micrographs of GM-HL were obtained by means of a negative-staining method. Sample solutions of GM-HL were mixed with a 4% aqueous solution of ammonium molybdate. The sample was then applied to a carbon grid and dried overnight in a vacuum desiccator at room temperature. The electron micrographs were taken on an electron microscope (JEM-100SX, JEOL, Tokyo, Japan).

Therapeutic Experiment of GM-HL *in Vivo* All animal experiments were approved by the committee of the Center for Animal Resources and Development, Kumamoto University, Japan. Eight-week-old mdx mice, which have a stop codon TAA in exon23 of the dystrophin gene, were intraperitonealy injected with either GM-HL, GM alone or HL. The given dosages of GM were 1× (34 mg/kg/d), 5× (170 mg/kg/d), and 10× (340 mg/kg/d). The number of mice for GM-HL 1×, GM-HL 5×, GM-HL 10×, GM 1×, GM 10×, HL 1×, HL 5×, and control (non-treated) were 3, 2, 1, 3, 7, 3, 2, and 5, respectively. After 2 weeks of the injection (3 times/d), the skeletal muscles were isolated, and the blood samples were collected from the treated mice. The efficiency of dystrophin positive fibers was calculated by the average number of dystrophin positive fibers in 3 randomly chosen photographs of dystrophin immunostaining skeletal muscle tissues per mouse. The creatine kinase (CK) and creatinine levels of each mouse were measured by a laboratory examination agency (SRL, Tokyo, Japan).

Immunochemical Staining of Dystrophin and Histological Analysis Skeletal muscles from gastrocnemius of treated mdx mice were frozen in isopentane pre-cooled in liquid nitrogen and 10-μm-thick sections were cut with a cryostat. The expression of dystrophin was analyzed with mouse monoclonal anti-dystrophin antibody (DYS2; 1 : 25, Novacastra Laboratories, Newcastle, U.K.) and biotinylated anti-mouse immunoglobulin G (IgG) reagent (VECTOR M.O.M. Immunodetection Kit, Vector Laboratories, Burlingame, CA, U.S.A.) as the secondary antibody. The immunoreactivity was visualized using 3,3′-diaminobenzidine as the chromogen substrate. The average number of dystrophin positive fibers was counted on 3 photographs that were randomly taken per mouse.

Confocal Laser Microscopy The accumulation of fluorescence-labeled HL (NBD-HL)[24] to the skeletal muscle was observed using confocal laser microscopy (CLM). NBD-HL were intraperitonealy injected into normal (B10, 8-week-old) and mdx mice. After the injection, the skeletal muscles (gastrocnemius) were isolated from the mice each time (1, 2, 6 h). The dissected muscles were embedded in an OCT compound and rapidly frozen. The cryosections of each muscle were made and stained with TO-PRO-3 dye (Invitrogen, Carlsbad, CA, U.S.A.) solution including an antifade reagent (0.5% 1,4-di-azobicyclo-(2,2,2)-octane) for detecting the cell nucleus. The sections were observed using CLM (TCS-SP, Leica Microsystems, Wetzlar, Germany) with 488 nm Ar laser line for NBDPC detection (emission; 500—600 nm) and 633 nm He–Ne laser line for TO-PRO-3 detection (emission; 640—703 nm). The biodistribution of NBD-HL to the organs of mdx mice was also observed using CLM. NBD-HL were intravenously injected into the mdx mice. After 1 h of the injection, the organs (brain, lung, liver, heart, kidney, spleen and skeletal muscle) were isolated from the mice. The dissected organs were embedded in an OCT compound and their cryosections were stained with TO-PRO-3 and observed using CLM as described above.

Auditory Brainstem Response (ABR) Female (8-week-old, $n=1$) and male (8-week-old, $n=7$) mdx mice were treated with GM-HL 10× and GM 10× for 14 d, respectively. After 2 weeks of the intraperitoneal (i.p.) injection (3 times/d), the hearing ability was determined by the auditory brainstem response (ABR).[25] ABR was obtained from mice anesthetized with a mixture of nitrous oxide/oxygen (1 : 1) gas and 3% halothane. Responses were differentially recorded between subcutaneous stainless steel electrodes at the vertex (active) and mastoid (reference), and the lower back served as ground. Testing was performed in a sound-attenuated box. The ABR, response to the sound of clicks, were recorded using a signal processor (Neuropack μ, Nihon Kohden, Tokyo, Japan).

Statistical Analysis Statistical analysis was performed by Student's t-test. A confidence level $p<0.05$ was considered significant.

RESULTS

Morphology of HL, GM-HL and NBD-HL Morphologies of HL, GM-HL and NBD-HL were examined on the basis of dynamic light scattering measurements and electron microscopy. The hydrodynamic diameters (d_{hy}) of HL, GM-HL and NBD-HL were almost the same sizes of 60—90 nm with a narrow range of size distribution (Fig. 1A). The diameters remained stable for more than 4 weeks. An electron micrograph of GM-HL showed the presence of spherical vesicles with a diameter of 60—90 nm as shown in Fig. 1B.

Accumulation of HL to Muscle Cells *in Vivo* The accumulation of NBD-HL to the skeletal muscle cells of normal (B10) and mdx mice *in vivo* was observed using CLM. The results are shown in Fig. 2. The green fluorescence of NBD-HL was detected in the cytoplasm and cytoplasmic membranes of myofibers of normal and mdx mice. Interestingly, the NBD-HL accumulated more in the cytoplasmic membranes of mdx mice (Fig. 2B) after 1 h of the i.p. injection as compared with those of normal mice (Fig. 2A). Then,

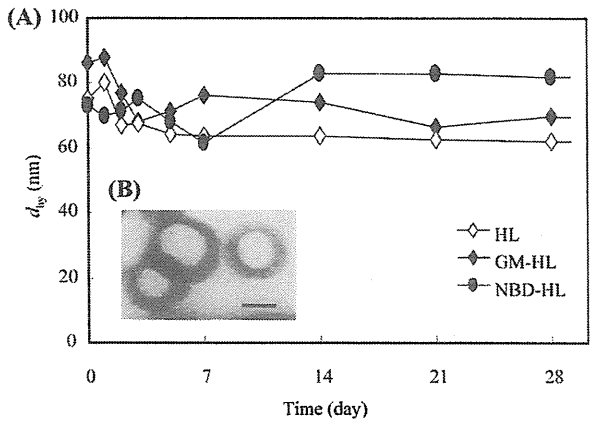

Fig. 1. Morphology of HL, GM-HL and NBD-HL

(A) Time courses of hydrodynamic diameters (d_{hy}) change for HL, GM-HL and NBD-HL prepared by sonication method. The d_{hy} of HL, GM-HL and NBD-HL were measured using a light scattering spectrometer at 25 °C. HL and GM-HL: [DMPC]=30 mM, [$C_{12}(EO)_{23}$]=1.58 mM, [GM]=10 mg(potency)/ml. NBD-HL: [DMPC]=10 mM, [$C_{12}(EO)_{23}$]=0.549 mM, [NBDPC]=0.439 mM. (B, inset) An electron micrograph of GM-HL by a negative staining method. [DMPC]=10 mM, [$C_{12}(EO)_{23}$]=0.526 mM, [GM]=3.33 mg(potency)/ml. Scale bar: 50 nm.

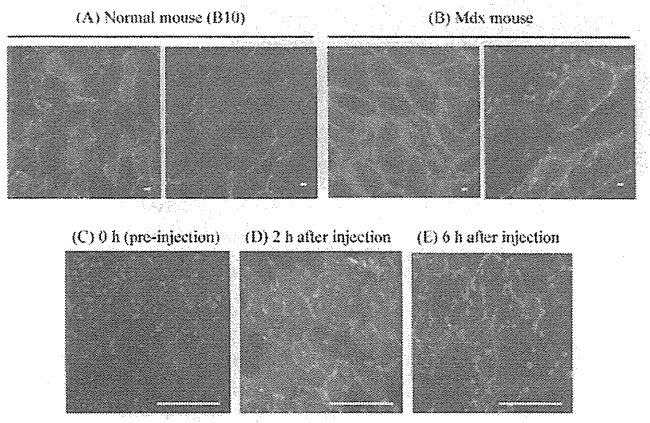

Fig. 2. Fluorescence Micrographs of Skeletal Muscle Cells for Normal and Mdx Mice after the i.p. Injection of NBD-HL

After the i.p. injection of NBD-HL into normal (B10) and mdx mice, the skeletal muscles were isolated from the mice, the cryosections of each muscle were stained with TO-PRO-3, and the stained sections were observed using CLM. Green: NBD-HL, Red: TO-PRO-3. (A) Normal and (B) mdx mice after 1 h of the injection of NBD-HL. Mdx mice after (C) 0 h (pre-injection), (D) 2 h and (E) 6 h of the injection of NBD-HL. Dose: [DMPC]=67.98 mg/kg, [$C_{12}(EO)_{23}$]=6.59 mg/kg, [NBDPC]=3.76 mg/kg. Scale bar: (A) (B) 10 μm, (C) (D) (E) 100 μm.

we investigated the retention time of NBD-HL in the myofibers of mdx mice. The higher fluorescence intensity of NBD-HL was observed in the myofibers of mdx mice after 2 h of the i.p. injection (Fig. 2D) compared with that of pre-injection (Fig. 2C). Furthermore, the fluorescence intensity of NBD-HL was consecutively observed after 6 h of the injection (Fig. 2E).

Therapeutic Effects of GM-HL on Mdx Mice *in Vivo*

The therapeutic effects of GM-HL on mdx mice were investigated *in vivo*. Generally, the CK level indicates the degree of muscle necrosis and the average CK level of mdx mice (control) in this experiment was 4239±501.1 (IU/l) as shown in Fig. 3. On the other hand, after 2 weeks of the i.p. injection, the average CK levels of GM-HL 1×, 5×, and 10× injected mdx mice decreased to 685±140 (IU/l), 759±122 (IU/l) and 610 (IU/l), respectively. The average CK levels of GM 1×

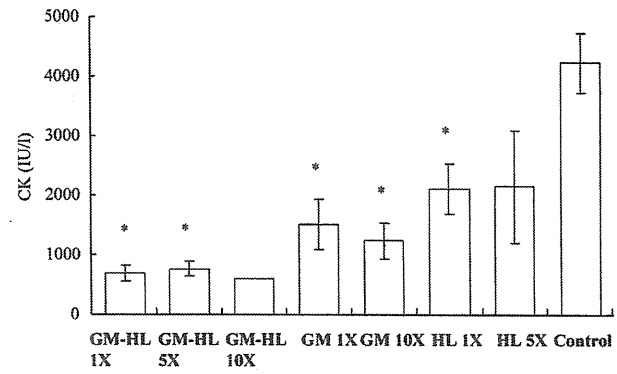

Fig. 3. CK Level in Blood of Mdx Mice after the Treatment with GM-HL, GM and HL

After 2 weeks of injection (3 times/d), the blood was collected from the treated mdx mice and the creatine kinase (CK) level of each mouse was measured. Data represent the mean±S.E. (n=1-6). Control means a CK level of the untreated mdx mice. Dose: GM-HL 1×: [DMPC]=694.0 mg/kg/d, [$C_{12}(EO)_{23}$]=64.39 mg/kg/d, [GM]=34 mg/kg/d, GM-HL 5×: [DMPC]=3470 mg/kg/d, [$C_{12}(EO)_{23}$]=322.0 mg/kg/d, [GM]=170 mg/kg/d, GM-HL 10×: [DMPC]=6940 mg/kg/d, [$C_{12}(EO)_{23}$]=643.9 mg/kg/d, [GM]=340 mg/kg/d, GM 1×: [GM]=34 mg/kg/d, GM 10×: [GM]=340 mg/kg/d, HL 1×: [DMPC]=694.0 mg/kg/d, [$C_{12}(EO)_{23}$]=64.39 mg/kg/d, HL 5×: [DMPC]=3470 mg/kg/d, [$C_{12}(EO)_{23}$]=322.0 mg/kg/d. * Significant difference (p<0.05) compared with control.

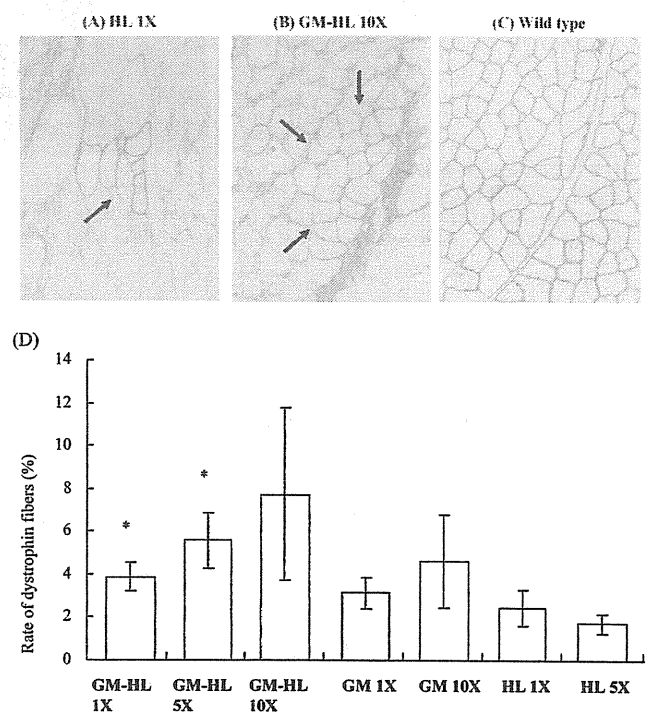

Fig. 4. Expression of Dystrophin in Skeletal Muscle Tissues of Mdx Mice after the Treatment with GM-HL, GM and HL

After 2 weeks injection (3 times/d), skeletal muscles were isolated from the treated mice and the expression of dystrophin was analyzed with mouse monoclonal anti-dystrophin antibody and biotinylated anti-mouse IgG reagent. The immunoreactivity was visualized using 3,3′-diaminobenzidine and the average number of dystrophin positive fibers was counted on 3 photographs that were randomly taken per mouse. Dystrophin immunostaining of skeletal muscle tissues was isolated from (A) HL 1× treated mdx mice, (B) GM-HL 10× treated mdx mice and (C) untreated normal mice (Wild type). (D) Rate of dystrophin positive fiber in skeletal muscle tissues of GM-HL, GM and HL treated mdx mice. * Significant difference (p<0.05) compared with HL 5×. Dose: GM-HL 1×: [DMPC]=694.0 mg/kg/d, [$C_{12}(EO)_{23}$]=64.39 mg/kg/d, [GM]=34 mg/kg/d, GM-HL 5×: [DMPC]=3470 mg/kg/d, [$C_{12}(EO)_{23}$]=322.0 mg/kg/d, [GM]=170 mg/kg/d, GM-HL 10×: [DMPC]=6940 mg/kg/d, [$C_{12}(EO)_{23}$]=643.9 mg/kg/d, [GM]=340 mg/kg/d, GM 1×: [GM]=34 mg/kg/d, GM 10×: [GM]=340 mg/kg/d, HL 1×: [DMPC]=694.0 mg/kg/d, [$C_{12}(EO)_{23}$]=64.39 mg/kg/d, HL 5×: [DMPC]=3470 mg/kg/d, [$C_{12}(EO)_{23}$]=322.0 mg/kg/d.

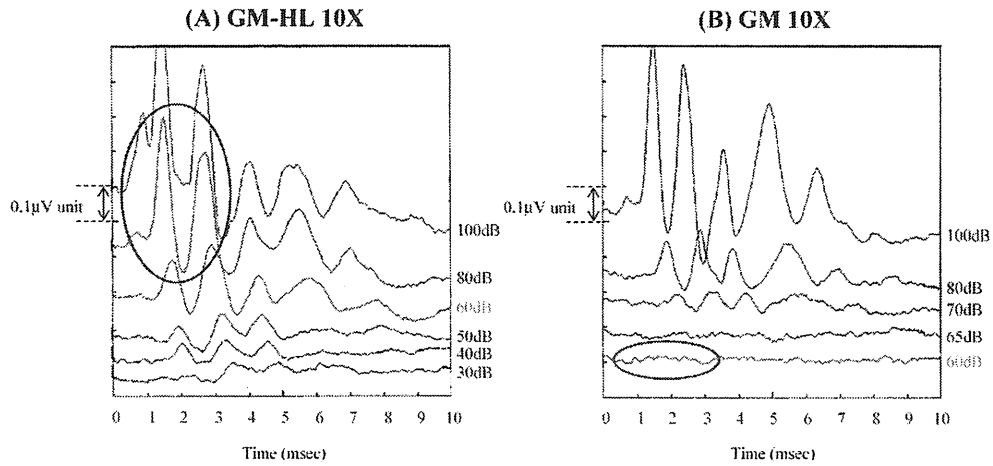

Fig. 5. ABR of Mdx Mice Treated with GM-HL 10× and GM 10×

After 2 weeks of i.p. injection of (A) GM-HL 10× and (B) GM 10× in to the mdx mice (3 times/d), the ABR was obtained from anesthetized mice in a sound-attenuated box. The responses were differentially recorded between subcutaneous stainless steel electrodes at the vertex (active) and mastoid (reference), and the lower back served as ground using a signal processor. Dose: GM-HL 10×: [DMPC]=6940 mg/kg/d, $[C_{12}(EO)_{23}]$=643.9 mg/kg/d, [GM]=340 mg/kg/d, GM 10×: [GM]=340 mg/kg/d.

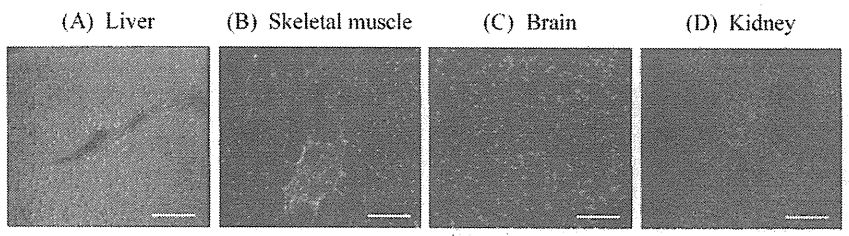

Fig. 6. Biodistribution of NBD-HL in Mdx Mice after i.v. Injection *in Vivo*

After 1 h of i.v. injection of NBD-HL into mdx mice, the organs were isolated from the mice. The dissected organs of (A) liver, (B) skeletal muscle, (C) brain and (D) kidney were stained with TO-PRO-3 and the sections were observed using CLM. Green: NBD-HL, Red: TO-PRO-3. Dose: [DMPC]=67.98 mg/kg, $[C_{12}(EO)_{23}]$=6.59 mg/kg, [NBDPC]=3.76 mg/kg. Scale bar: 100 μm.

and 10× were 1521±422 (IU/l) and 1237±293 (IU/l), respectively. The average CK levels of HL 1× and 5× were 2114±430 (IU/l) and 2145±955 (IU/l), respectively. The CK levels of GM-HL injected mdx mice showed a decreasing tendency in comparison with those of HL and GM alone. The total CK levels of GM-HL (1× and 5×), GM (1× and 10×) and HL 1× significantly decreased in comparison with that of control ($p<0.05$). Furthermore, the dystrophin immunostaining of skeletal muscle tissues of mdx mice indicated that the dystrophin positive fibers were well observed in GM-HL 10× injected mice (Fig. 4B) as compared with HL 1× injected mice (Fig. 4A). The rate of dystrophin positive fibers of GM-HL 1×, GM-HL 5×, GM-HL 10×, GM 1×, GM 10×, HL 1×, and HL 5× were 3.87±0.676%, 5.58±1.31%, 7.73±4.01%, 3.13±0.718%, 4.62±2.17%, 2.44±0.835%, and 1.74±0.450%, respectively as shown in Fig. 4D. The efficiency of dystrophin positive fibers in the GM-HL 10× injected group was the highest followed by the GM-HL 5× injected group. The rates of dystrophin positive fibers for GM-HL (1× and 5×) were significantly higher than that for HL 5× ($p<0.05$).

Suppression of the Ototoxicity of GM by Using GM-HL The ototoxicity of GM-HL on the mdx mice was evaluated by ABR tests *in vivo*. As shown in Fig. 5, the ABR of the mdx mice after the injection of GM-HL 10× was observed to 30 dB, though that after the injection of GM 10× was observed only to 70 dB. The ABR of GM-HL 10× injected mdx mice was normal as observed in the wave of 60 dB, while that of GM 10× injected mice was abnormal as observed in the wave of 60 dB and as being almost flat. Furthermore, the biodistribution of NBD-HL in mdx mice after the intravenous (i.v.) injection was examined using CLM. In the organs of brain, liver, kidney, intestine, skeletal muscle and spleen, the accumulation of NBD-HL was observed in the liver (Fig. 6A) and skeletal muscle (Fig. 6B) of mdx mice after 1 h of the injection. No accumulation of NBD-HL was detected in other organs including the brain (Fig. 6C) and kidney (Fig. 6D).

DISCUSSION

Pharmacological approaches for DMD with promising candidates for using drugs such as aminoglycoside antibiotics, calcium blokers, steroids, *etc.* are under investigation. Some of them have been effective for animal models. However, they are not enough to improve the muscle weakness for patients. One of these reasons is that the effective dose as a medicine is not injected to patients because of the severe side effects. For the reduction of the side effects, several DDS utilizing nanopolymers[26] and viral vectors[27] *etc.* were reported for the treatment of DMD. However, there were very few reports to achieve the more selective delivery to dystrophic muscles comparing with normal muscles.

In this study, we investigated the effects of DDS using HL

composed of DMPC and $C_{12}(EO)_{23}$ as a carrier of GM for DMD therapy *in vivo*. It is very important to clarify the characteristics such as the size, shape and stability of liposomes in DDS. So, we prepared HL including GM and examined the morphology of GM-HL on the basis of dynamic light scattering measurements and electron microscopy. The hydrodynamic diameters of HL, GM-HL and NBD-HL were 60—90 nm, which remained stable for over 4 weeks (Fig. 1). It is worthy to note that GM-HL having 60—90 nm in diameter could avoid the reticuloendothelial system *in vivo*.[28] Next, we observed the accumulation of NBD-HL in skeletal muscles of mdx and normal mice *in vivo* using CLM and demonstrated that HL could accumulate more to myofibers of mdx mice as compared with those of normal mice (Figs. 2A, B) and retained in the cells at least 6 h after the injection (Fig. 2E). Significantly, the increasing dystrophin positive fibers in skeletal muscle cells (Fig. 4) and decreasing CK levels (Fig. 3) in the blood of mdx mice were observed after the treatment with GM-HL. It is suggested that GM should be carried more efficiently into the muscular cells of mdx mice by HL. These results indicate that GM-HL could be more effective for DMD therapy than GM alone. Furthermore, we evaluated the ototoxicity of GM-HL on the mdx mice by ABR tests and the results indicated that GM-HL 10× suppressed the ototoxicity in mdx mice (Fig. 5). In addition, the serum creatinine concentrations of GM-HL injected mdx mice were normal (data not shown), suggesting that GM-HL could suppress nephrotoxicity. Three of 4 GM 10× injected mice lost 1—2 g of weight, while the GM-HL 10× injected mice gained weight (data not shown). It is attractive that HL-GM have not only more therapeutic effects but also less side effects as compared with GM alone. Finally, we examined the biodistribution of HL in mdx mice *via* i.v. injections *in vivo* in order to investigate the possibility of clinical applications in the future. The accumulation of NBD-HL was observed in the liver and skeletal muscle in comparison with other organs after 1 h of the i.v. injection (Figs. 6A, B). Especially, the accumulation was hardly observed in brain (Fig. 6C) and kidney (Fig. 6D). In the previous paper, we indicated the same biodistribution of NBD-HL except skeletal muscle in the normal mice.[29] These results suggest that HL could be metabolized in liver, and the toxicities of GM to kidney and auditory nerve systems could be suppressed by using HL as the drug carrier.

The first advantage of using HL as DDS is that this system could reduce toxicity. The second one is that the dosage could be stable for more than 4 weeks. The third one is that it could allow an escape from the reticuloendothelial system. The results obtained in this study suggest that the DDS with HL could be applied in the novel therapy using GM for patients with DMD.

Acknowledgements The authors thank Ryan Pruchnic (Cook MyoSite, Pittsburgh, Penn) for his assistance. This work was supported in part by Grant-in-Aids for Science Research from the Ministry of Education, Culture, Sports, Science and Technology of Japan (Nos. 20107007, 20360377, 20560732, 19560782, 21560813, 19591209) and a Research Grant (19-7) for nervous and mental disorders from the Ministry of Health, Labour, and Welfare.

REFERENCES

1) Hoffman E. P., Brown R. H. Jr., Kunkel L. M., *Cell*, **51**, 919—928 (1987).
2) Koenig M., Hoffman E. P., Bertelson C. J., Monaco A. P., Feener C., Kunkel L. M., *Cell*, **50**, 509—517 (1987).
3) Gillard E. F., Chamberlain J. S., Murphy E. G., Duff C. L., Smith B., Burghes A. H. M., Thompson M. W., Sutherland J., Oss I., Bodrug S. E., Klamut H. J., Ray P. N., Worton R. G., *Am. J. Hum. Genet.*, **45**, 507—520 (1989).
4) Forrest S. M., Cross G. S., Flint T., Speer A., Robson K. J., Davies K. E., *Genomics*, **2**, 109—114 (1988).
5) Lindlöf M., Kiuru A., Kääriäinen H., Kalimo H., Lang H., Pihko H., Rapola J., Somer H., Somer M., Savontaus M. L., de la Chapelle A., *Am. J. Hum. Genet.*, **44**, 496—503 (1989).
6) Prior T. W., Wenger G. D., Papp A. C., Snyder P. J., Sedra M. S., Bartolo C., Moore J. W., Highsmith W. E., *Hum. Mutat.*, **5**, 263—268 (1995).
7) Mendell J. R., Buzin C. H., Feng J., Yan J., Serrano C., Sangani D. S., Wall C., Prior T. W., Sommer S. S., *Neurology*, **57**, 645—650 (2001).
8) Howard M., Frizzell R. A., Bedwell D. M., *Nat. Med.*, **2**, 467—469 (1996).
9) Howard M. T., Shirts B. H., Petros L. M., Flanigan K. M., Gesteland R. F., Atkins J. F., *Ann. Neurol.*, **48**, 164—169 (2000).
10) Barton-Davis E. R., Cordier L., Shoturma D. I., Leland S. E., Sweeney H. L., *J. Clin. Invest.*, **104**, 375—381 (1999).
11) Welch E. M., Barton E. R., Zhuo J., Tomizawa Y., Friesen W. J., Trifillis P., Paushkin S., Patel M., Trotta C. R., Hwang S., Wilde R. G., Karp G., Takasugi J., Chen G., Jones S., Ren H., Moon Y. C., Corson D., Turpoff A. A., Campbell J. A., Conn M. M., Khan A., Almstead N. G., Hedrick J., Mollin A., Risher N., Weetall M., Yeh S., Branstrom A. A., Colacino J. M., Babiak J., Ju W. D., Hirawat S., Northcutt V. J., Miller L. L., Spatrick P., He F., Kawana M., Feng H., Jacobson A., Peltz S. W., Sweeney H. L., *Nature* (London), **447**, 87—91 (2007).
12) PTC THERAPEUTICS. "Ataluen for Genetic Disorders." ⟨http://www.ptcbio.com/3.1.1_genetic_disorders.aspx⟩.
13) Ueoka R., Moss R. A., Swarup S., Matsumoto Y., Strauss G., Murakami Y., *J. Am. Chem. Soc.*, **107**, 2185—2186 (1985).
14) Ueoka R., Matsumoto Y., Moss R. A., Swarup S., Sugii A., Harada K., Kikuchi J., Murakami Y., *J. Am. Chem. Soc.*, **110**, 1588—1595 (1988).
15) Kitamura I., Kochi M., Matsumoto Y., Ueoka R., Kuratsu J., Ushio Y., *Cancer Res.*, **56**, 3986—3992 (1996).
16) Matsumoto Y., Kato T., Suzuki H., Hirose S., Naiki Y., Hirashima M., Ueoka R., *Bioorg. Med. Chem. Lett.*, **10**, 2617—2619 (2000).
17) Tanaka Y., Goto K., Matsumoto Y., Ueoka R., *Int. J. Pharm.*, **359**, 264—271 (2008).
18) Matsumoto Y., Kato T., Iseki S., Suzuki H., Nakano K., Iwahara M., Ueoka R., *Bioorg. Med. Chem. Lett.*, **9**, 1937—1940 (1999).
19) Ueoka R., Matsumoto Y., Ichihara H., Kiyokawa T., "Chemotherapy with Hybrid Liposomes Composed of Dimyristoylphosphatidylcholine and Polyoxyethylenealkyl Ether without Drugs," ACS Symposium Series 830, Biological Systems Engineering, Chap. 14, ed. by Marten M. R., Park T. H., Nagamune T., Am. Chem. Soc. Books, Washington, 2002, pp. 177—189.
20) Matsumoto Y., Iwamoto Y., Matsushita T., Ueoka R., *Int. J. Cancer*, **115**, 377—382 (2005).
21) Ichihara H., Nagami H., Kiyokawa T., Matsumoto Y., Ueoka R., *Anticancer Res.*, **28**, 1187—1196 (2008).
22) Komizu Y., Matsumoto Y., Ueoka R., *Bioorg. Med. Chem. Lett.*, **16**, 6131—6134 (2006).
23) Nakashima K., Miyagi M., Goto K., Matsumoto Y., Ueoka R., *Yakugaku Zasshi*, **124**, 231—235 (2004).
24) Nakano K., Iwamoto Y., Takata W., Matsumoto Y., Ueoka R., *Bioorg. Med. Chem. Lett.*, **12**, 3251—3254 (2002).
25) Hakuba N., Koga K., Gyo K., Usami S., Tanaka K., *J. Neurosci.*, **20**, 8750—8753 (2000).
26) Williams J. H., Schray R. C., Sirsi S. R., Lutz G. J., *BMC Biotechnol.*, **8**, 35—47 (2008).
27) Gregorevic P., Blankiship M. J., Allen J. M., Crawford R. W., Meuse L., Miller D. G., Russell D. W., Chamberlain J. S., *Nat. Med.*, **10**, 828—834 (2004).
28) Allen T. M., Hansen C., Martin F., Redemann C., Yau-Young A., *Biochem. Biophys. Acta*, **1066**, 29—36 (1991).
29) Ichihara H., Nagami H., Yamamoto K., Matsumoto Y., Ueoka R., *Yakugaku Zasshi*, **123**, 25—34 (2003).